

# A MECHANISTIC MODEL OF IRON CARBONATE FILM GROWTH AND THE EFFECT ON CO<sub>2</sub> CORROSION OF MILD STEEL

Srdjan Nestic\*, Kun-Lin John Lee\* and Vukan Ruzic  
Department of Mechanical Engineering  
The University of Queensland  
Brisbane Queensland, Australia

## ABSTRACT

A model of iron carbonate (FeCO<sub>3</sub>) film growth is proposed, which is an extension of the recent mechanistic model of CO<sub>2</sub> corrosion by Nestic et al. <sup>1</sup>. In the present model the film growth occurs by precipitation of iron carbonate once saturation is exceeded. The kinetics of precipitation is dependent on temperature and local species concentrations which are calculated by solving the coupled species transport equations. Precipitation tends to build up a layer of iron carbonate on the surface of the steel and reduce the corrosion rate. On the other hand, the corrosion process induces voids under the precipitated film thus increasing the porosity and leading to a higher corrosion rate. Depending on the environmental parameters such as temperature, pH, CO<sub>2</sub> partial pressure, velocity, etc, the balance of the two processes can lead to a variety of outcomes. Very protective films and low corrosion rates are predicted at high pH, temperature, CO<sub>2</sub> partial pressure and Fe<sup>2+</sup> ion concentration due to formation of dense protective films as expected.

The model has been successfully calibrated against limited experimental data. Parametric testing of the model has been done in order to gain insight into the effect of various environmental parameters on iron carbonate film formation. The trends shown in the predictions agreed well with the general understanding of the CO<sub>2</sub> corrosion process in the presence of iron carbonate films. The present model confirms that the concept of scaling tendency is a good tool for predicting the likelihood of protective iron carbonate film formation.

---

\* Current address: NSF I/U CRC Corrosion and Multiphase Flow, Ohio University, Stocker Center, Athens, OH.

## INTRODUCTION

The recent mechanistic model of Nesic et al.<sup>1</sup> covers most of the important processes present in uniform CO<sub>2</sub> corrosion of carbon steel: electrochemical reactions at the steel surface, chemical reactions and transport of species between the steel surface and the bulk solution including transport through the porous corrosion film. The physical, mathematical and numerical aspects of the model are explained in detail in the original paper, however a very brief outline is given below to facilitate the understanding of the present model.

Since it is a model of uniform corrosion, a one-dimensional computational domain is used, stretching from the steel surface through the pores of a surface film and the mass transfer boundary layer, ending in the turbulent bulk of the solution, as sketched in Figure 1. The concentration of each species is governed by a species conservation (mass balance) equation. A universal form of the equation which describes transport for species  $j$  in the presence of chemical reactions, which is valid both for the liquid boundary layer and the porous film, is:

$$\underbrace{\frac{\partial(\varepsilon c_j)}{\partial t}}_{\text{accumulation}} = \underbrace{\frac{\partial}{\partial x} \left( \varepsilon^{1.5} D_j^{eff} \frac{\partial c_j}{\partial x} \right)}_{\text{net flux}} + \underbrace{\varepsilon R_j}_{\substack{\text{source or sink} \\ \text{due to chemical reactions}}} \quad (1)$$

where  $c_j$  is the concentration of species  $j$ ,  $\varepsilon$  is the porosity of the film,  $D_j^{eff}$  is the effective diffusion coefficient of species  $j$  (which includes both the molecular and the turbulent component),  $R_j$  is the source or sink of species  $j$  due to all the chemical reactions in which the particular species is involved,  $t$  is time and  $x$  is the spatial coordinate. It should be noted that in the transport equation above, turbulent convection has been replaced by turbulent diffusion and electromigration has been neglected. The boundary conditions are: in the bulk - equilibrium concentrations of species, at the steel surface - a flux of species is determined from the rate of the electrochemical reactions (equal to zero for non-electroactive species).

Even if the original model of Nesic et al.<sup>1</sup> is mechanistic and offers an insight into the various complex processes occurring in CO<sub>2</sub> corrosion - from a practical point of view it is just another worst-case CO<sub>2</sub> corrosion prediction model. Admittedly, it does go one step further than other similar CO<sub>2</sub> models as it enables prediction of conditions leading to protective film formation, as well as the effect of protective films once they are in place. However, there is a missing link: it cannot predict the kinetics of film growth, neither can it predict the morphology of the growing films. The present study aims at filling these gaps, i.e. it uses the mechanistic model of Nesic et al.<sup>1</sup> as a basis and extends it to cover the film growth process.

In the text below, the physical mathematical and numerical aspects of the film growth model are discussed first. This is followed by a section discussing the verification of the model done by comparing the predictions with measurements. Finally a section is included where the new model is used to study the effects of various parameters affecting the film growth process and the effects on the corrosion rate.

## THE FILM GROWTH MODEL

In CO<sub>2</sub> corrosion of carbon steel, when the concentrations of Fe<sup>2+</sup> and CO<sub>3</sub><sup>2-</sup> ions exceed the solubility limit, they can precipitate to form solid iron carbonate according to:



When iron carbonate precipitates at the steel surface, it can slow down the corrosion process by presenting a diffusion barrier for the species involved in the corrosion process but also by blocking (covering) a portion of the steel surface and preventing the underlying steel from further dissolution.

Iron carbonate film growth depends primarily on the precipitation rate  $R_{FeCO_3}$ . As more iron carbonate precipitates the film grows in density as well as thickness. However, the steel surface corrodes under the film, continuously creating a “void” between the film and the steel surface (here called “film undermining”). As soon as it is created the void starts filling by the ongoing precipitation. When the rate of precipitation at the steel surface equals or exceeds the rate of corrosion (film undermining) dense protective films form - sometimes very thin but still protective. Vice versa when the corrosion process undermines the newly formed film faster than precipitation can fill in the voids, a porous and unprotective film forms - which can be sometimes very thick. This phenomenon has been previously quantified through the use of a non-dimensional parameter termed “scaling tendency”<sup>5</sup>:

$$ST = \frac{R_{FeCO_3}}{CR} \quad (3)$$

which describes the relative rates of precipitation and corrosion expressed in the same volumetric units. For  $ST \ll 1$  porous and unprotective films are likely to form, and conversely when  $ST \geq 1$  conditions become favorable for formation of dense protective iron carbonate films. However, the use of scaling tendency is not as straightforward as it appears. Strictly speaking one needs to compute the scaling tendency at the steel surface where the films form (surface scaling tendency -  $SST$ ). Therefore one needs information about the solution chemistry at the steel surface which can be very different from the one in the bulk, particularly if some sort of surface film is already in place (e.g. iron carbide, mill scale). Further, the scaling tendency changes with time as the corrosion and precipitation rate change. The model shown below does not explicitly use the concept of scaling tendency even if the physical processes underlying it (precipitation and undermining) are accounted for. The surface and bulk scaling tendencies are computed in the model in order to check their validity as effective indicators of protective film formation.

The proposed equation describing the film growth kinetics is rather simple: it is a mass balance for the solid iron carbonate:

$$\underbrace{\frac{\partial c_{FeCO_{3(s)}}}{\partial t}}_{\text{local change}} = \underbrace{R_{FeCO_{3(s)}}}_{\text{precipitation rate}} - CR \underbrace{\frac{\partial c_{FeCO_{3(s)}}}{\partial x}}_{\text{undermining rate}} \quad (4)$$

expressing the fact that the amount of solid iron carbonate found at any location,  $c_{FeCO_{3(s)}}$  in  $\text{kmol/m}^3$  will increase over time because of precipitation and/or will decrease due to the undermining effect.

The last term on the rhs in equation (4) above needs a clarification. Corrosion of the steel causes the steel surface shown in Figure 1 to move to the left. Within the framework of a fixed grid (in space) this is a moving boundary problem. If the whole domain is to be covered at all times, it appears that the fixed grid needs to be continuously extended to the left in order to “cover” the voids created by the corrosion process. This is not easy and would require a lot of interpolation and complex bookkeeping. Another

simpler option is to assume that the grid is “attached” to the steel surface which is moving to the left with a velocity equal to the corrosion rate  $CR$ . The advantage of this option is that in this case one does not have to keep extending the grid. However, in a moving frame of reference it appears as if the whole computational domain shown in Figure 1 moves to right, as corrosion proceeds. In other words, a convective-like term appears in all the transport equations (1) for the species as well as in equation (4) for solid iron carbonate. This term appears to sweep everything away from the steel surface with a velocity  $CR$  what has the same effect as the surface of the steel moving in the opposite direction with the same velocity. Hence the convective-like term appears on rhs of equation (4) describing the film undermining effect\*.

Another aspect of equation (4) deserves a comment. Physically, precipitation of crystalline films (such as iron carbonate) goes through two phases: nucleation and crystal growth. In most cases when there is a solid steel surface present, with all its imperfections being good candidates for nuclei formation, the nucleation phase is over relatively fast and can be disregarded. It can be assumed that the rate of precipitation is controlled by the crystal growth rate. Generally crystals grow from a large number of discrete nuclei into dendritic structures which may or may not join, forming a porous film. A discrete lattice growth modelling approach has been employed in the past to model the film growth process<sup>6-8</sup>. However, for the purposes of the present model, it would be computationally costly and mathematically difficult to model a three-dimensional discrete film growth process and couple it to the existing one-dimensional transport model for all the other species. It seemed more appropriate to persist with the one-dimensional control volume approach in describing the film growth as expressed by equation (4). In a control volume approach, all properties are assumed to be constant within a control volume and therefore it appears that some detailed information about the film can be lost - smeared over the control volume. This can be avoided by using very fine grids - small control volume sizes of the order of  $\Delta x \propto 10^{-7}$  m which is still a few orders of magnitude larger than the length scale of the dendrites. In this way it can be assumed that any averaging of the film properties across such small control volumes will not lead to a significant loss of detailed information. After all, the present model is not aimed at elucidating the fine points of crystalline iron carbonate film growth, but attempts to capture the overall effect these films have on the  $CO_2$  corrosion process.

It is convenient to express the morphology of iron carbonate films via the distribution of volumetric porosity  $\varepsilon$  since it is used as the principal film parameter affecting transport of species. Tortuosity and permeability of the film which appear in the original transport equation have already been expressed in terms of porosity (see equation 1)<sup>1</sup>. Volumetric porosity is defined as:

$$\varepsilon = \frac{V_{void}}{V_{total}} = \frac{(V_{total} - V_{FeCO_3(s)})}{V_{total}} = 1 - \frac{V_{FeCO_3(s)}}{V_{total}} \quad (5)$$

Rearranging film growth equation (4) to express it in terms of porosity yields:

$$\frac{\partial \varepsilon}{\partial t} = - \frac{M_{FeCO_3(s)}}{\rho_{FeCO_3(s)}} R_{FeCO_3(s)} - CR \frac{\partial \varepsilon}{\partial x} \quad (6)$$

---

\* The sweeping effect is not very significant for transport of the dissolved species in the solution as the sweeping velocity  $CR$  is at least a few orders of magnitude smaller than the “diffusional velocity” and negligible when compared to convection. For example a corrosion rate of the order of 1 mm/y amounts to a sweeping velocity of the order of 1 nm/min. Diffusional velocity for a typical species in the solution is of the order of 1 mm/min.

where  $M_{FeCO_3(s)} = 115.847$  kg/kmol is the molecular mass and  $\rho_{FeCO_3(s)} = 3900$  kg/m<sup>3</sup> is the density of iron carbonate.

The rate of precipitation  $R_{FeCO_3(s)}$  in equation (6) can be described as a function of supersaturation  $S$ , the solubility limit  $K_{sp}$ , temperature  $T$  and surface area-to-volume ratio  $A/V$ :

$$R_{FeCO_3(s)} = \frac{A}{V} \cdot f(T) \cdot K_{sp} \cdot f(S) \quad (7)$$

Supersaturation is defined as:

$$S = \frac{c_{Fe^{2+}} \cdot c_{CO_3^{2-}}}{K_{sp}} \quad (8)$$

From the two different expressions describing the kinetics of iron carbonate precipitation proposed by Johnson and Tomson<sup>4</sup> and Van Hunnik et al.<sup>5</sup>, the latter is used in conjunction with the film growth model, because it is believed to give more realistic results especially at higher supersaturation.

Within the context of the present model, the surface area-to-volume ratio  $A/V$  is defined locally - as a function of the film porosity in a particular control volume. The two studies mentioned above<sup>4,5</sup> offered no guidance on what values for  $A/V$  to use in such a case. Using simple asymptotic analysis it can be deduced that in the bulk solution where there is no film,  $\varepsilon=1$  and  $A/V=0$ . Implicitly this means that homogeneous precipitation in the bulk solution does not occur no matter how high the local supersaturation and temperature. On the other end of the  $\varepsilon$  scale, in 100% dense films,  $\varepsilon=0$  and  $A/V=0$ . In between these extremes, for  $0<\varepsilon<1$  the surface area-to-volume ratio can become very large. There is some information in the open literature on how  $A/V$  changes with porosity<sup>9,10</sup> based on simple geometrical models which usually fail at one of the extremes. After much trial and error, by using geometrical as well as physical arguments, and through comparison with CO<sub>2</sub> corrosion experiments (described below), it has been concluded that the area-to-volume ratio can be expressed as a function of porosity in the following form:

$$\frac{A}{V} \propto \frac{\varepsilon^2(1-\varepsilon)}{\Delta x} \quad (9)$$

where  $\Delta x$  is the width of the control volume.

## THE NUMERICAL MODEL

The film growth equation (6) was discretized using a finite difference method. An explicit time discretization scheme was used to simplify the coupling with the rest of the model which was discretized fully implicitly in order to maintain stability. This can easily be justified by the wide disparity of the time scales: relaxation time for the species transport equations (1) is of the order of seconds while the for the film growth equation (6) it is of the order of hours or even days. In other words film precipitation happens so slowly, compared to the other processes in CO<sub>2</sub> corrosion, that it can be calculated by using an explicit time discretization scheme without risking instability.

In equation (6), the film undermining term  $CR \cdot \partial \varepsilon / \partial x$  is of a convective nature as discussed previously. A first order upwinding method is commonly used (in lieu of central differences) for spatial discretization of convective terms in order to achieve numerical stability. However, in the absence of any physical diffusion (iron carbonate films do not diffuse) simple upwinding leads to large numerical diffusion and unacceptable level of numerical errors. This is due to the hyperbolic nature of equation (6) and the very small  $CFL$  number ( $CFL = CRA\Delta t / \Delta x \approx 10^{-3}$ ). Exact solution of hyperbolic equations is obtained only for  $CFL = 1$ .<sup>11,12</sup> Therefore, a more accurate Koren's flux limiter scheme<sup>13</sup> was used to discretize the film undermining term.

A typical initial condition for equation (6) used below was  $\varepsilon = 1$  throughout the solution - i.e. a case with no initial film, although any other porosity profile could have been used instead to simulate the presence of a preformed carbide film or a mill scale. Boundary conditions for equation (6) were  $\varepsilon = 0$  at the steel surface and  $\varepsilon = 1$  in the bulk solution.

All the results of the simulations shown below were numerically tested by rigorously performing temporal and spatial grid refinement studies. The data shown in the figures below are all grid and time step independent (within acceptable tolerances). Uniform control volume size and time steps were used to improve the order of accuracy of the interpolation schemes.

## COMPARISON WITH EXPERIMENTS

In order to verify and “fine-tune” the performance of the model described above, accurate  $\text{CO}_2$  corrosion experiments in the presence of iron carbonate films were needed. There is a number of such experiments found in the open literature, however upon closer inspection all had to be rejected, because there was some relevant information which was not reported in each of them. Therefore custom designed glass cell experiments were conducted using a rotating cylinder electrode. Conditions were chosen to enable rapid protective iron carbonate film formation in a relatively short time frame (one-two days), so that the reproducibility of the measurements could be easily established.

### Experimental setting and procedure

The glass cell was filled up with 2.5 liters of electrolyte which was made up of distilled water and 1.0 wt% sodium chloride. At the beginning, the solution was deaerated by bubbling  $\text{CO}_2$  gas for 1 hour. The cell was sealed tightly to prevent oxygen contamination, and  $\text{CO}_2$  gas bubbling was continued throughout the experiment, hence it can be assumed that water vapor and  $\text{CO}_2$  were the only gas constituents. Subsequently the solution was heated to  $80^\circ\text{C}$ . Since the cell was operating at atmospheric pressure, partial pressure of  $\text{CO}_2$  was approximately 0.54 bar. The desired pH of 6.6 was then adjusted by adding sodium hydrogen carbonate ( $\text{NaHCO}_3$ ). A cylindrical 1020 mild steel specimen with a ferritic-pearlitic microstructure was sanded using 1000 grit silicon carbide (SiC) paper, then washed with ethanol and dried before immersion into the solution. The rotating speed of the cylindrical specimen was adjusted to give the peripheral velocity of the steel surface of 1 m/s. The electrochemical corrosion measurements were performed by using a potentiostat connected to a PC. The corrosion rate was measured every hour using the linear polarization resistance (LPR) method, by polarizing the working electrode  $\pm 5$  mV vs. the open circuit potential at a rate of 0.1 mV/s. The polarization constant  $b$  was determined to be 17 mV by using the simplified electrochemical model of Nescic et al.<sup>14</sup>. This procedure of determining the  $b$  value was frequently verified with weight loss and was found to be accurate within  $\pm 15\%$ . At the end of the experiment, after the specimen was removed from the cell it was immediately rinsed with ethanol in order

to avoid film contamination with oxides. It was then allowed to dry and mounted in a low viscosity epoxy resin in order to fix the film. The specimen was cross sectioned, polished, platinum coated and observed using Scanning Electron Microscopy (SEM) and Energy Dispersive Spectroscopy (EDS).

### Comparison case #1

In Figure 2 measured and predicted corrosion rates are compared for an experiment conducted at atmospheric pressure, temperature  $T=80^{\circ}\text{C}$ , pH 6.6, partial pressure of  $\text{CO}_2$   $P_{\text{CO}_2}=0.54$  bar, velocity  $v=1$  m/s. In order to form protective  $\text{FeCO}_3$  films via precipitation in a short time frame, steel wool was placed at the bottom of the glass cell at the very beginning of the experiment in order to provide an ample source of  $\text{Fe}^{2+}$  ions. Based on pH 6.26 (measured once the pH reading stabilized with the steel wool in the cell), it was estimated via equilibrium calculations that the bulk concentration of  $\text{Fe}^{2+}$  was approximately 250 ppm leading to a bulk supersaturation  $S=576$  and a surface scaling tendency of  $SST=9.7$  at the steel surface prior to any film formation. As expected under these conditions, the corrosion rate was reduced rapidly as protective iron carbonate films formed. The experiment was stopped after 10 hours when the corrosion rate was lower than 0.03 mm/year. The agreement between measured and predicted values shown in Figure 2 is very good given the complexity of the processes involved. In order to achieve such agreement the only freely adjustable parameter in the model was the unknown proportionality constant between the surface area-to-volume ratio and the porosity of the film in equation (9). The resulting relationship is depicted in Figure 3, suggesting that the internal surface area of the porous film grows rapidly as the film develops, reaching over  $1000 \text{ m}^2/\text{m}^3$  and then gradually reduces as the pores fill up with iron carbonate.

The predicted film growth process is shown in Figure 4 as a change of porosity in each control volume (layer of the film) with respect to time. It can be seen that the porosity decrease i.e. film buildup is initially sharpest in the first layer directly adjacent to the steel surface what is to be expected as nucleation can only happen there and also because highest supersaturation is reached at the steel surface. However as the steel surface corrodes under the film and undermines it, the second layer away from the steel surface experiences fastest film buildup, followed by the third layer etc., as the film grows in thickness. After 10 hours a very dense and protective film is formed close to the steel surface. Since the bulk supersaturation is very high the film would keep on growing. It is interesting to note that the first layer adjacent to the steel surface never reached the same high density of the other layers above it due to the undermining effect by corrosion.

Another probably more intuitive way of looking at the same film growth process is depicted in Figure 5. There, a change of porosity of the film is shown in time and space by using different shades of gray, black depicting a 100% dense ( $\varepsilon=0$ ) iron carbonate film and white meaning no film ( $\varepsilon=1$ ). Under the given conditions the film thickness changes approximately in a parabolic fashion with time as predicted by simple theory, however this is not always the case, as will be illustrated below.

Scanning Electron Microscopy (SEM) image of the cross section of the steel specimen from the experiment described above (exposed for 10 hours) is shown in Figure 6. When comparing the film thickness and morphology with the predicted values (highlighted by the rectangle in Figure 5) it is seen that the agreement is good for the thickness of film (measured: 4-6 $\mu\text{m}$ , predicted: 3.7  $\mu\text{m}$ ). Indeed the SEM image shows a fairly uniformly dense film with a more porous layer of iron carbonate adjacent to the steel surface, as predicted. It should be noted that during the experiment less than 1  $\mu\text{m}$  of steel was lost to the corrosion process.

## Comparison case #2

The next test of the model was to compare its performance using a different set of environmental conditions. It was particularly interesting to evaluate if the newly established relationship between the surface area-to-volume ratio and the porosity of the film depicted in Figure 3 would apply without adjustment - what would build confidence in its generality. A second set of experiments used for verification was conducted under the same condition as the previous set ( $T=80^{\circ}\text{C}$ ,  $\text{pH } 6.6$ ,  $P_{\text{CO}_2}=0.54$  bar,  $v=1$  m/s ) with the exception of the steel wool which was not used - resulting in a much lower  $\text{Fe}^{2+}$  concentration. Using equilibrium calculations, based on  $\text{pH } 4.6$  measured at the beginning of the experiment, it was estimated that the  $\text{Fe}^{2+}$  concentration was approximately 5-10 ppm throughout most of the experiment. The value of  $\text{pH}$  was adjusted to 6.6 by adding  $\text{NaHCO}_3$  what resulted in a bulk supersaturation  $S=10-23$  and a surface scaling tendency of  $SST=0.25-0.47$  prior to any film formation. Base on the high supersaturation it was expected that some precipitation would occur however, the low value of the surface scaling tendency suggested that the film could have troubles attaching to the surface.

The experiment was stopped after two days without achieving protective film formation. In Figure 7 measured and predicted corrosion rate were compared and both show that no protective films were formed after 48 hours. The agreement is rather good given that no adjustment of the model was made. In Figure 8 the prediction showed that some precipitation occurred, however the film layers adjacent to the rapidly corroding steel surface remained very porous due to the undermining effect while a more dense film grew at some distance away from the steel surface. The same is shown in Figure 9 showing that a relatively dense film formed at approximately 5-10  $\mu\text{m}$  away from the surface after 48 hours of exposure. Qualitatively this agreed well with the cross section examination conducted by using SEM, as shown in Figure 10, where a totally detached layer of iron carbonate can be seen approximately 10-20  $\mu\text{m}$  away from the steel surface. During the experiment approximately 10  $\mu\text{m}$  of steel was lost to the corrosion process.

Clearly one can be satisfied with the qualitative predictions obtained with the model. Not all of the predicted quantities agreed well enough with the experiments (e.g. film thickness) suggesting that some more fine-tuning is needed, requiring a new set of dedicated  $\text{CO}_2$  corrosion experiments conducted under a variety of environmental conditions leading to iron carbonate film growth. This is a task for the immediate future.

## PARAMETRIC TESTING

In this section the model will be used to predict  $\text{CO}_2$  corrosion under broadly varying environmental conditions in order to establish its more general applicability. No direct comparisons with experiments will be made in this section, however performance of the model will be contrasted against the general understanding of the  $\text{CO}_2$  corrosion process in the presence of iron carbonate films. As shown in the previous section (comparison case #1), the model was successful in predicting  $\text{CO}_2$  corrosion and film formation in an experiment conducted at  $T=80^{\circ}\text{C}$ ,  $\text{pH}=6.6$ ,  $P_{\text{CO}_2}=0.54$  bar,  $c_{\text{Fe}^{2+}}=250$  ppm,  $v=1$  m/s, and therefore this set of conditions will be used as a baseline case when varying the different parameters, one at a time.



## The effect of pH

It was shown previously both experimentally<sup>15</sup>, and computationally<sup>16</sup> that pH has a strong influence on the conditions leading to the formation of iron carbonate films. High pH results in a decreased solubility of iron carbonate, increased supersaturation and consequently higher precipitation rate and surface scaling tendency. In TABLE 1 the predicted supersaturation, scaling tendency, film thickness and a corrosion rate after 30 hours of exposure at various pH are shown. Judging by the high supersaturation alone, one could expect that protective film should form in all cases, given that the temperature is relatively high (80°C). However the surface scaling tendency seems to suggest that protective film formation might be very difficult at pH 5.8 (as  $SST < 1$ ) and probably sluggish at pH 6.0 ( $SST \approx 1$ ). The predictions of the corrosion rate at varying pH confirmed this as shown in Figure 11. At pH 5.8 the corrosion rate is not reduced by a significant amount after 30 hours reflecting the fact that a relatively porous, detached and unprotective film formed as shown in Figure 12. A clear trend can be observed in Figure 11: higher pH resulted in faster formation of more protective films, as expected. From Figure 12 one can deduce that as the pH was increased the resulting film was of similar thickness but progressively became more dense and protective, particularly in the vicinity of the steel surface.

## The effect of temperature

It is known that increased temperature aids iron carbonate film formation by accelerating the kinetics of precipitation. The predicted temperature effect on CO<sub>2</sub> corrosion is illustrated in Figure 13 for the baseline case (temperatures below 50°C are not shown as no film could be detected). Prior to any film formation the corrosion rate increases with temperature as expected. While very protective films formed rapidly at 80°C, already at 65°C and 55°C the kinetics of film formation was very much slower, while at 50°C it was so slow that only some very porous film formation can be detected. It is rather striking how under certain conditions a difference of 5°C can lead to two very different corrosion outcomes. At 55°C iron carbonate films form which offer good protection while at 50°C there is a detached, porous layer of iron carbonate film which offers little protection. Calculated data shown in TABLE 2 support this conclusion, where very high supersaturation is obtained at all temperatures, however the surface scaling tendency is significantly smaller than unity only at 50°C. By looking at Figure 14 it can be seen that the predicted film thickness does not vary much with temperature, however the film formed at 55°C is more porous particularly close to the metal surface due to the undermining effect than one formed at 65°C. At 80°C a very dense and thick protective film is obtained.

## The effect of CO<sub>2</sub> partial pressure

In the case of film-free CO<sub>2</sub> corrosion, an increase of CO<sub>2</sub> partial pressure ( $P_{CO_2}$ ) typically leads to an increase in the corrosion rate. However, when other conditions are favourable for formation of iron carbonate films, increased  $P_{CO_2}$  can help. At a constant pH, higher  $P_{CO_2}$  leads to an increase in CO<sub>3</sub><sup>2-</sup> concentration and a higher supersaturation (given the pH is high enough), what accelerates precipitation and film formation. The effect of  $P_{CO_2}$  on the corrosion rate in the presence of iron carbonate precipitation is illustrated in Figure 15 for the baseline case. Prior to film formation, increased  $P_{CO_2}$  leads to a rapid rise in corrosion rate. However, protective films form rapidly in all cases, even for the lowest  $P_{CO_2} = 0.54$  bar (given the pH 6.6 and high Fe<sup>2+</sup> concentration). An increase in  $P_{CO_2}$  leads to formation of even more protective films - and this happens faster. Data are presented only for the first 5 hours of corrosion as very low, almost indistinguishable corrosion rates are obtained beyond. One could expect

such behaviour just by looking at the high supersaturations and scaling tendencies shown in TABLE 3. By inspecting Figure 16 it can be concluded that somewhat denser and clearly thicker films form at higher  $P_{CO_2}$ .

#### The effect of $Fe^{2+}$ concentration

The concentration of  $Fe^{2+}$  ions in the solution ( $c_{Fe^{2+}}$ ) is another important factor that contributes to film formation. The increase of  $c_{Fe^{2+}}$  results in higher supersaturation, which consequently accelerates the precipitation rate and leads to higher surface scaling tendency. In Figure 17 the effect of  $c_{Fe^{2+}}$  on the rate of corrosion rate reduction due to iron carbonate film formation is shown for the baseline case. The  $c_{Fe^{2+}}$  does not affect the corrosion rate if there is no iron carbonate film (at  $t=0$ ). At  $c_{Fe^{2+}}=5\text{ppm}$ , supersaturation is achieved however the surface scaling tendency is much less than unity (see TABLE 4) and one cannot expect protective films to form. This is confirmed as the corrosion rate is not reduced significantly even after 30 hours (see Figure 17). The iron carbonate film which forms is very porous and unprotective (see Figure 18 but also the comparison case #2 - Figure 7 - Figure 10). At higher concentrations more protective films form as shown in Figure 17 and. Figure 18.

#### The effect of velocity

Higher velocity is directly associated with higher turbulence and more effective mixing in the solution. This affects both the corrosion rate of the bare steel surface and the precipitation rate of iron carbonate. Prior to any film formation, high velocity leads to increased corrosion rate (see Figure 19) as the transport of cathodic species toward the steel surface is enhanced by turbulent transport. At the same time the transport of  $Fe^{2+}$  ions away from the steel surface is also increased, leading to a lower concentration of  $Fe^{2+}$  ions at the steel surface. This results in a lower surface supersaturation and slower precipitation rate (see TABLE 5). Both effects contribute to less protective films being formed at high velocities. Interestingly the model suggests that somewhat thicker films form at higher velocity however they are more porous particularly close to the metal surface (see Figure 20). This behavior could clearly be termed flow accelerated corrosion (FAC) even if no film dissolution or mechanical erosion is involved.

## CONCLUSIONS

- A mechanistic model of iron carbonate film growth in  $CO_2$  corrosion of carbon steel was created and coupled with the overall corrosion prediction model. The model relies on accurate prediction of the solution chemistry at the metal surface. It includes two principle mechanisms which determine the kinetics of growth and the resulting morphology of the iron carbonate films: precipitation and undermining of the film by ongoing corrosion. The morphology is described by the distribution of porosity throughout the film.
- The model is capable of predicting the kinetics of iron carbonate film growth, the change in morphology of the film with respect to space and time as well as the resulting corrosion rate time evolution.

- The model has been successfully calibrated against limited experimental data. Further adjustment of the model will be done as more accurate data on CO<sub>2</sub> corrosion in the presence of iron carbonate films emerge.
- Parametric testing of the model has been done in order to gain insight into the effect of various environmental parameters on iron carbonate film formation. The trends shown in the predictions agreed well with the general understanding of the CO<sub>2</sub> corrosion process in the presence of iron carbonate films.
- The present model confirms that the concept of scaling tendency is a good tool for predicting the likelihood of protective iron carbonate film formation. It was found that protective films formed when the surface scaling tendency was equal or larger than unity, otherwise porous and unprotective film formed irrespective of the level of supersaturation. If the bulk scaling tendency is used, the critical value is 0.6 - 0.7, what is close to the experimentally observed value by Van Hunnik et al.<sup>5</sup>.

### ACKNOWLEDGMENT

During this work, John Lee and Vukan Ruzic have been supported by an Australian Postgraduate Award and a scholarship from the Mechanical Engineering Department, University of Queensland, Australia. The authors are grateful for many useful comments and discussions with Arne Dugstad and Rolf Nyborg from IFE, Norway and Magnus Nordsveen from Scandpower, Norway, which helped in creating this model as it stands today.

### REFERENCES

1. S. Netic, M. Nordsveen R. Nyborg and A. Stangeland, "A Mechanistic Model for CO<sub>2</sub> Corrosion with Protective Iron Carbonate Films", CORROSION/2001, paper no. 40, (Houston, TX: NACE International, 2001).
2. J. S. Newman, Electrochemical Systems, 2<sup>nd</sup> Edition, (Prentice Hall, Englewood Cliffs, New Jersey, 1991).
3. J. W. Mullin, Crystallization, 3<sup>rd</sup> edition, (Oxford, 1993).
4. M. L. Johnson and M. B. Tomson, "Ferrous Carbonate Precipitation Kinetics and Its Impact on CO<sub>2</sub> Corrosion", CORROSION/91, paper no. 268, (Houston, TX: NACE International, 1991).
5. E. W. J. van Hunnik, B. F. M. Pots and E. L. J. A. Hendriksen, "The Formation of Protective FeCO<sub>3</sub> Corrosion Product Layers in CO<sub>2</sub> Corrosion". CORROSION/96, paper no. 6, (Houston, TX: NACE International, 1996).
6. I. Nainville, A. Lemarchand and J.P. Badiali, "Growth and morphology of thick films formed on a metallic surface", Electrochimica Acta, Vol41, No11/12, (1996): p. 1855.
7. M. Lafage, V. Russier and J.P. Badiali, "Simulation of growth and corrosion during the formation of a passive layer", Journal of Electroanalytical Chemistry, 450, (1998): p. 203.

8. A. Taleb, J. Stafiej, A. Chausse, R. Messina and J.P. Badiali, "Simulation of film growth and diffusion during the corrosion process", *Journal of Electroanalytical Chemistry*, 500, (2001): p. 554
9. Nakayama and F. Kuwahara, "Numerical Modeling of Convective Heat Transfer in Porous Media Using Microscopic Structures", *Handbook of Porous Media*. (Marcel Dekker Publication, New York, 1995).
10. L. Latour, P. Mitra, R. Kleinberg and C. Sotak, "Time-Dependent Diffusion Coefficient of Fluids in Porous Media as a Probe of Surface-to-Volume Ratio", *Journal of Magnetic Resonance. Series A* 101, (1993): p.342.
11. K. Hoffmann, S. Chiang, "Computational Fluid Dynamics for Engineers - Volume 1", fourth print, (A Publication of Engineering Education System, Kansas, USA, 1997).
12. B.P. Leonard, "A Stable and Accurate Convective Modelling Procedure based on Quadratic Upstream Interpolation", *Computer methods in applied mechanics and engineering*, 19, (1979): p. 59. (North-Holland Publishing Company, 1977).
13. B. Koren, "A robust upwind discretization method for advection, diffusion and source terms", *Numerical methods for advection-diffusion problems*, Vieweg, Braunschweig, (1993): p117.
14. S. Nestic, J. Postlethwaite, S. Olsen, *Corrosion*, 52, (1996): p. 280.
15. A. Dugstad, "The Importance of  $\text{FeCO}_3$  Supersaturation on the  $\text{CO}_2$  Corrosion of Carbon Steels. CORROSION/92, paper no. 14, (Houston, TX: NACE International, 1992).
16. S. Nestic, M. Nordsveen, R. Nyborg and A. Stangeland, "A Mechanistic Model for  $\text{CO}_2$  Corrosion of Mild Steel in the Presence of Protective Iron Carbonate Films - Part II: A Numerical Experiment.", under review, *Corrosion journal*, 2001.

TABLE 1.  
 PREDICTED SUPERSATURATION, SCALING TENDENCY, FILM THICKNESS AND  
 CORROSION RATE AT VARIOUS pH FOR T=80°C,  $P_{CO_2} = 0.54$  bar,  $c_{Fe^{2+}} = 250$  ppm,  $v=1$  m/s.

pH	Supersaturation (prior to any film formation)		Scaling Tendency (prior to any film formation)		Film thickness* (after 30 hours) in $\mu\text{m}$	Corrosion rate* (after 30 hours) in mm/y
	Surface	bulk	surface	Bulk		
5.8	63	11	0.41	0.06	6.2	1.6
6.0	154	29	1.03	0.18	4.9	0.13
6.26	464	104	3.03	0.66	4.8	0.04
6.6	1595	576	9.70	3.35	8.4	0.03

\* Film thickness as well as porosity are shown in Figure 12.

\* Corresponding corrosion rate vs. time curves are shown in Figure 11.

TABLE 2.  
 PREDICTED SUPERSATURATION, SCALING TENDENCY, FILM THICKNESS AND  
 CORROSION RATE AT VARIOUS TEMPERATURES FOR pH 6.6,  $P_{CO_2} = 0.54$  bar,  
 $c_{Fe^{2+}} = 250$  ppm,  $v=1$  m/s.

T in °C	Supersaturation (prior to any film formation)		Scaling Tendency (prior to any film formation)		Film thickness* (after 30 hours) in $\mu\text{m}$	Corrosion rate* (after 30 hours) in mm/y
	Surface	bulk	surface	Bulk		
50	562	245	0.43	0.19	4.9	1.16
55	675	290	0.76	0.32	5.1	0.3
65	969	387	2.22	0.87	5.1	0.06
80	1595	576	9.70	3.35	8.4	0.03

\* Film thickness as well as porosity are shown in Figure 14.

\* Corresponding corrosion rate vs. time curves are shown in Figure 13.

TABLE 3.  
 PREDICTED SUPERSATURATION, SCALING TENDENCY, FILM THICKNESS AND  
 CORROSION RATE AT VARIOUS CO<sub>2</sub> PARTIAL PRESSURES FOR T=80°C, pH 6.6,  
 $c_{Fe^{2+}}=250$  ppm, v=1 m/s.

$P_{CO_2}$ in bar	Supersaturation (prior to any film formation)		Scaling Tendency (prior to any film formation)		Film thickness* (after 5 hours) in $\mu$ m	Corrosion rate* (after 5 hours) in mm/y
	Surface	bulk	surface	Bulk		
0.54	1595	576	9.70	3.35	2.5	0.14
1	3078	1069	10.77	3.59	3.5	0.11
2	5881	2142	11.75	4.13	5.6	0.12
5	11800	5422	12.26	5.66	11.4	0.2

\* Film thickness as well as porosity are shown in Figure 16.

\* Corresponding corrosion rate vs. time curves are shown in Figure 15.

TABLE 4.  
 PREDICTED SUPERSATURATION, SCALING TENDENCY, FILM THICKNESS AND  
 CORROSION RATE AT VARIOUS Fe<sup>2+</sup> CONCENTRATIONS FOR T=80°C, pH 6.6,  
 $P_{CO_2} = 0.54$  bar, v=1 m/s.

$c_{Fe^{2+}}$ in ppm	Supersaturation (prior to any film formation)		Scaling Tendency (prior to any film formation)		Film thickness* (after 30 hours) in $\mu$ m	Corrosion rate* (after 30 hours) in mm/y
	Surface	bulk	surface	Bulk		
5	51	11	0.27	0.05	7.1	1.98
25	185	58	1.1	0.32	5.7	0.13
100	671	230	3.90	1.31	6.0	0.04
250	1595	576	9.70	3.35	8.4	0.03

\* Film thickness as well as porosity are shown in Figure 18.

\* Corresponding corrosion rate vs. time curves are shown in Figure 17.

TABLE 5.  
 PREDICTED SUPERSATURATION, SCALING TENDENCY, FILM THICKNESS AND  
 CORROSION RATE AT VARIOUS VELOCITIES FOR T=80°C, pH 6.6,  $P_{CO_2} = 0.54$  bar,  
 $c_{Fe^{2+}} = 250$  ppm.

v in m/s	Supersaturation (prior to any film formation)		Scaling Tendency (prior to any film formation)		Film thickness <sup>♦</sup> (after 10 hours) in $\mu$ m	Corrosion rate <sup>▼</sup> (after 10 hours) in mm/y
	Surface	bulk	surface	Bulk		
0.1	1770	576	10.6	3.4	3.5	0.06
1	1595	576	9.70	3.35	3.7	0.058
10	790	576	3.24	2.36	5.1	0.6
20	686	576	2.6	2.16	5.9	1.27

♦ Film thickness as well as porosity are shown in Figure 20.

▼ Corresponding corrosion rate vs. time curves are shown in Figure 19.

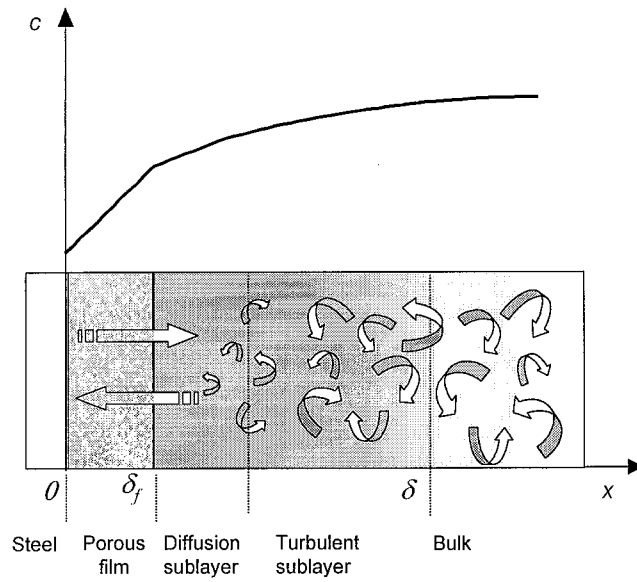


Figure 1. Sketch of the computational domain and a typical concentration profile for a dissolved species.



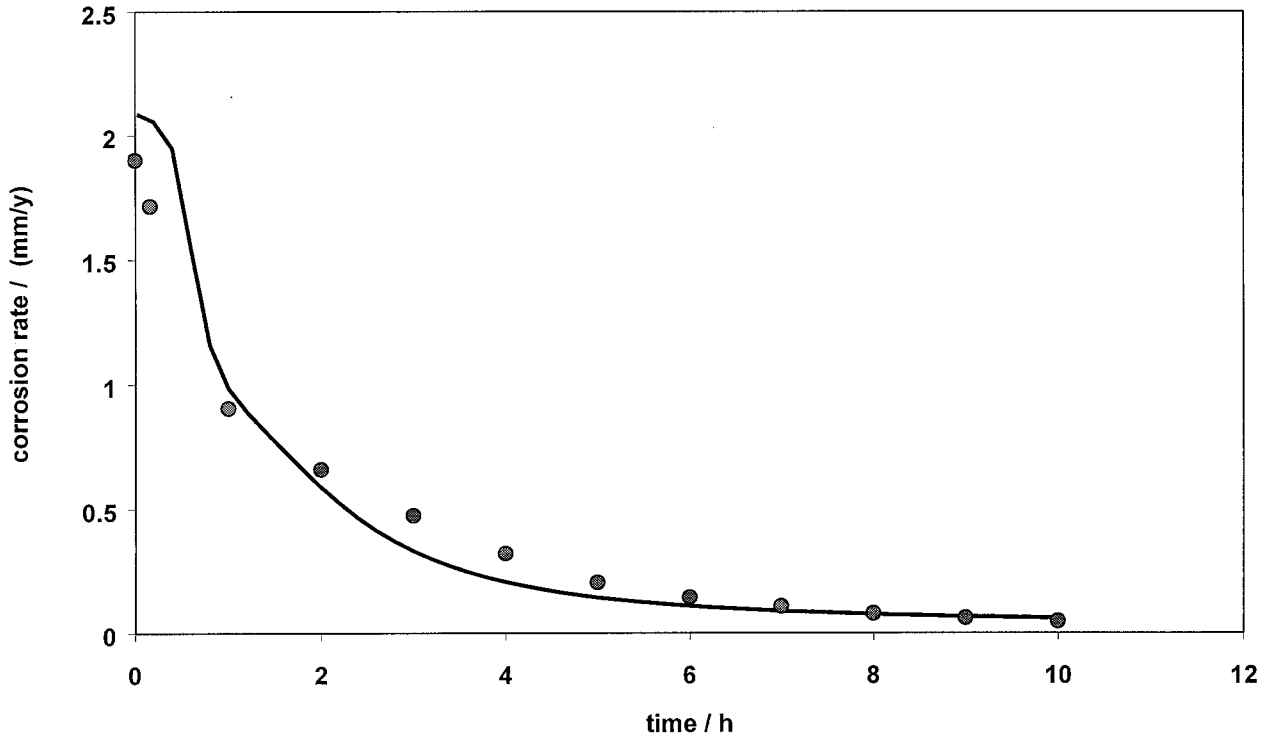


Figure 2. Comparison between experimental data (points) and model predictions (line) for  $T=80^{\circ}\text{C}$ ,  $\text{pH}$  6.6,  $P_{\text{CO}_2} = 0.54$  bar,  $c_{\text{Fe}^{2+}} = 250$  ppm,  $v=1$  m/s.

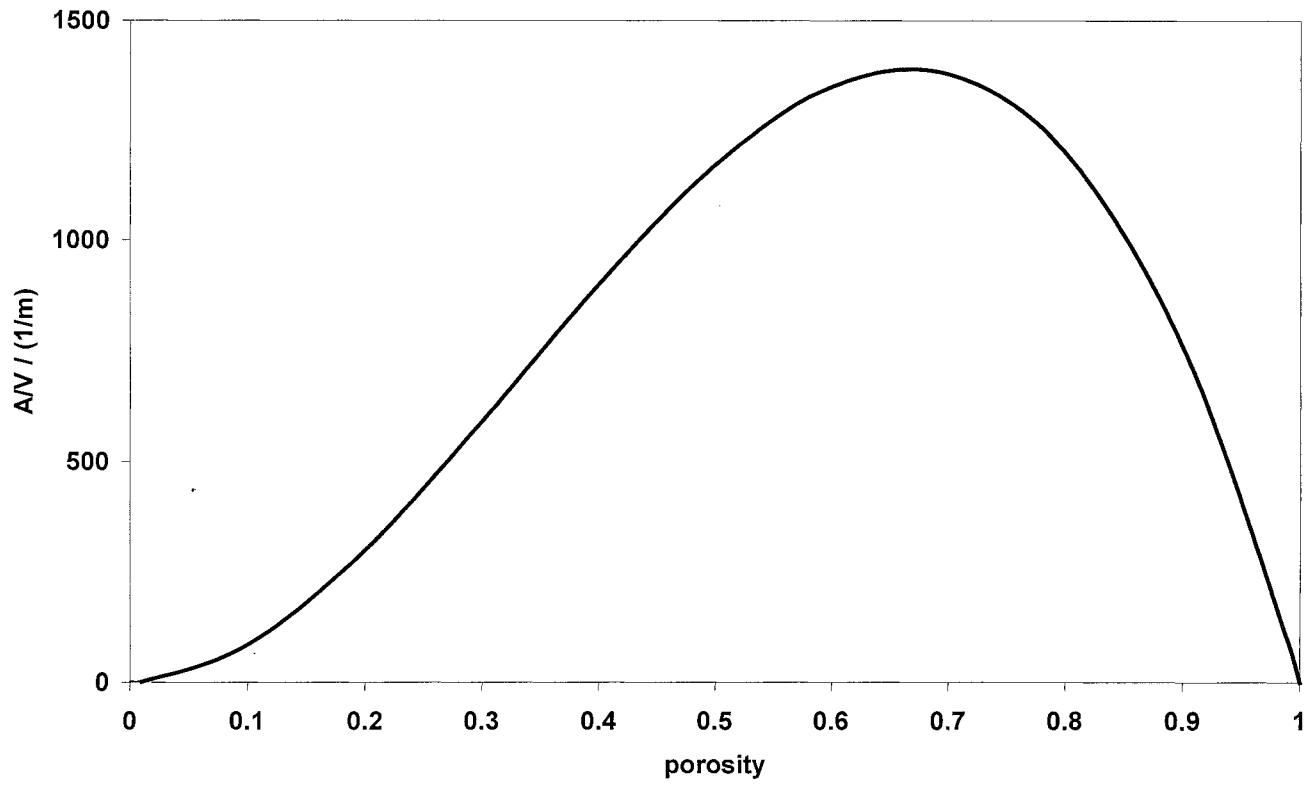


Figure 3. Surface area-to-volume ratio  $A/V$  as a function of porosity  $\varepsilon$  for a control volume of  $\Delta x \propto 10^{-7}$  m.

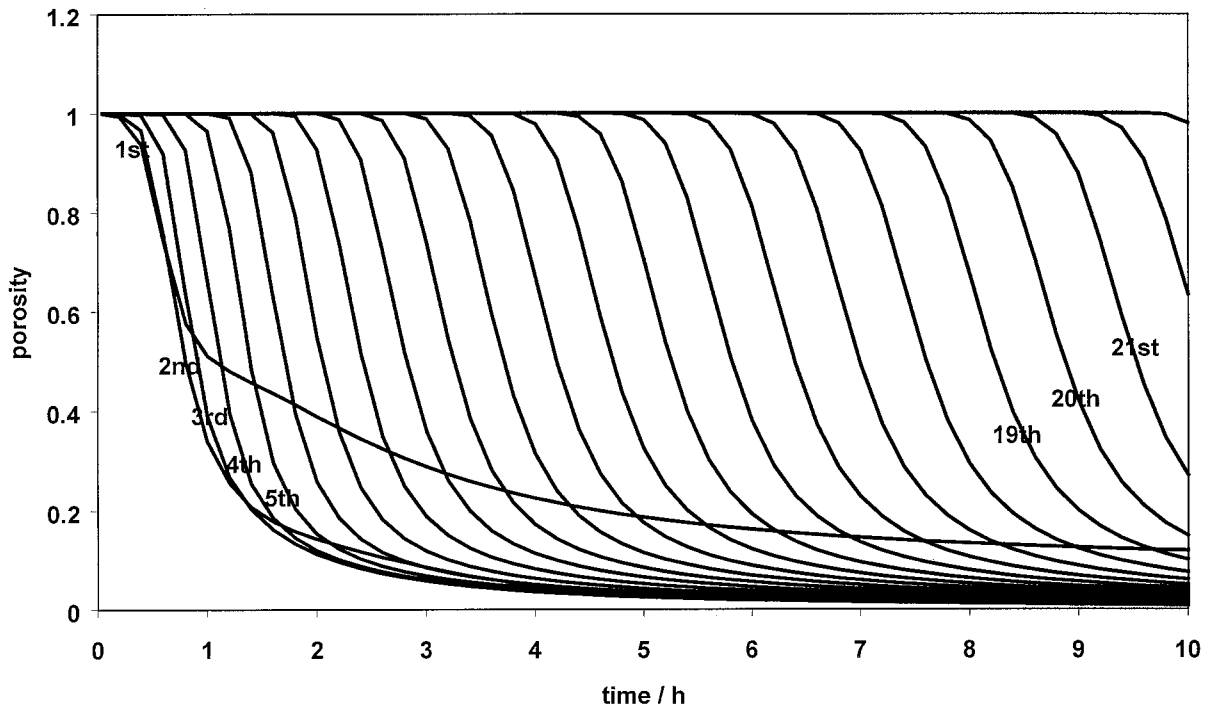


Figure 4. The predicted porosity change of different iron carbonate film layers with respect to time. Each layer is  $0.16 \mu\text{m}$  thick. Conditions:  $T=80^\circ\text{C}$ ,  $\text{pH } 6.6$ ,  $P_{\text{CO}_2} = 0.54 \text{ bar}$ ,  $c_{\text{Fe}^{2+}} = 250 \text{ ppm}$ ,  $v=1 \text{ m/s}$ .

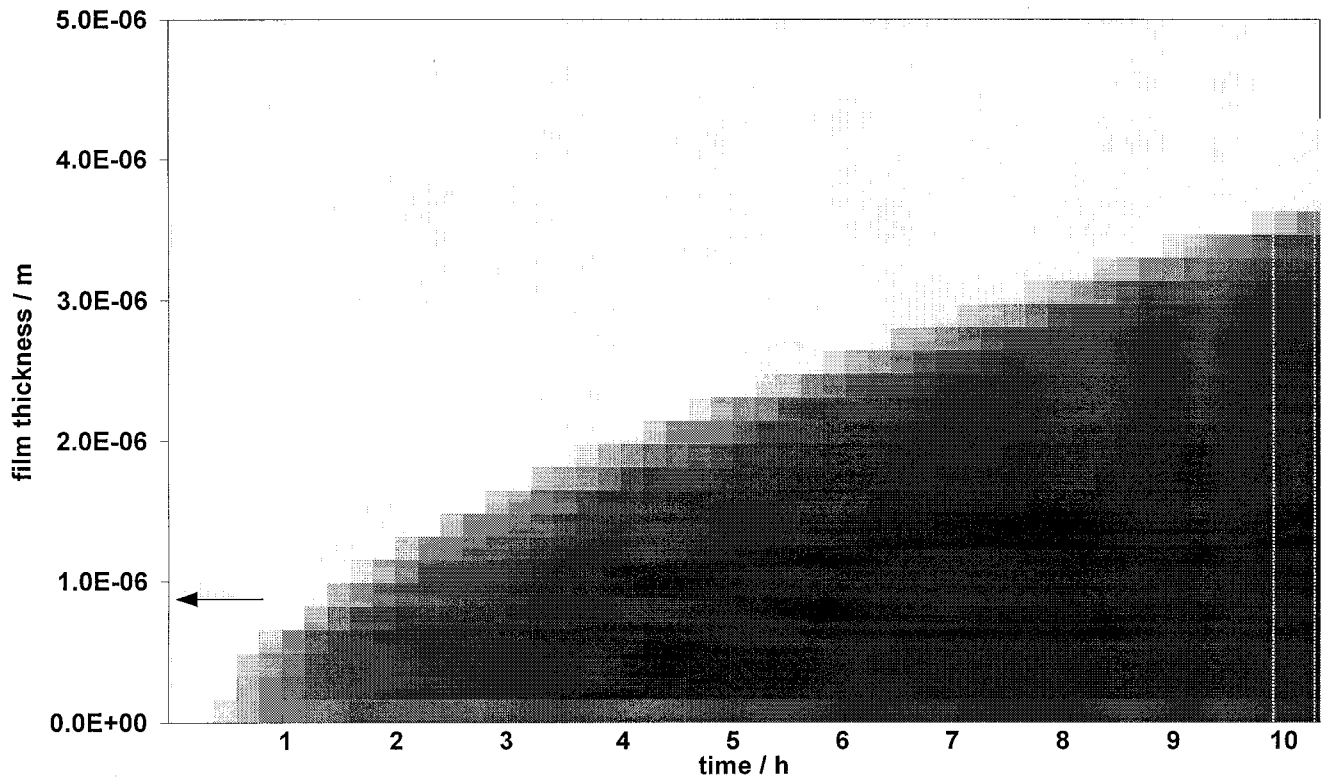


Figure 5. Predicted iron carbonate film growth with respect to time for  $T=80^{\circ}\text{C}$ ,  $\text{pH } 6.6$ ,  $P_{\text{CO}_2} = 0.54 \text{ bar}$ ,  $c_{\text{Fe}^{2+}} = 250 \text{ ppm}$ ,  $v=1 \text{ m/s}$ . Black depicts a 100% dense ( $\varepsilon=0$ ) iron carbonate film and white means no film ( $\varepsilon=1$ ). The arrow denotes the position of the steel surface at the beginning of the corrosion process ( $t=0$ ). The rectangle highlights the film obtained after 10 hours which is used for comparison with the experimentally observed film shown in Figure 6.

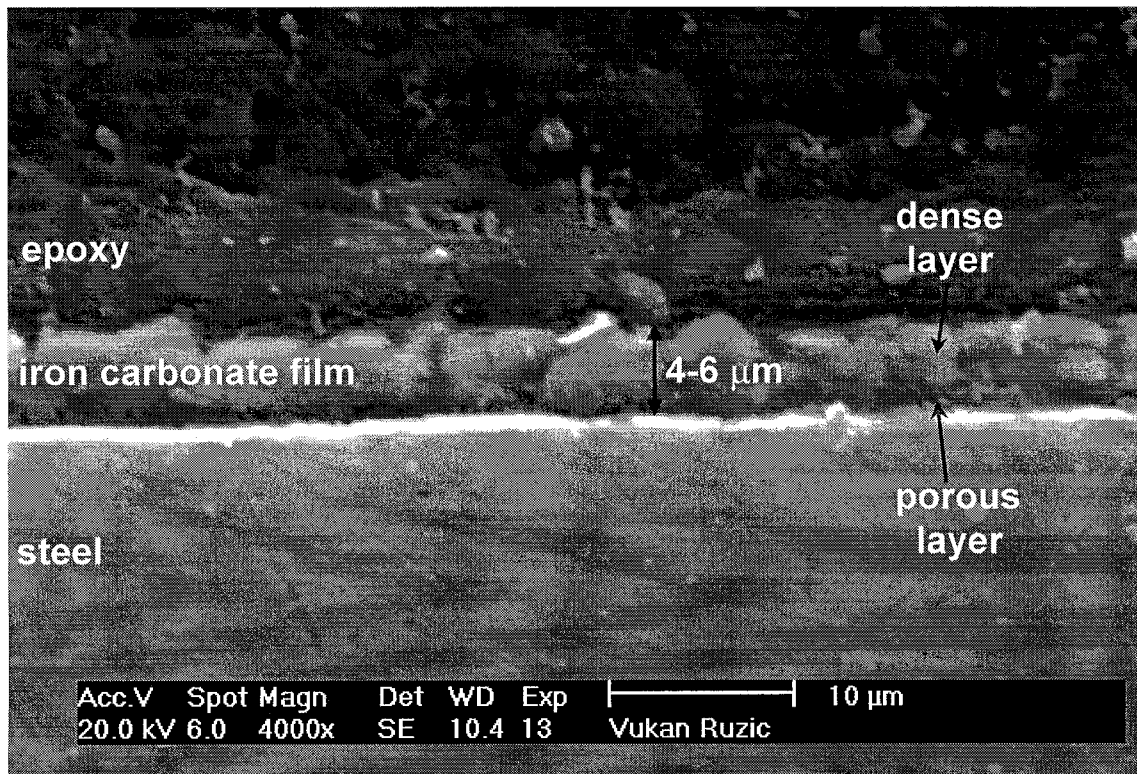


Figure 6. SEM image of a cross section of a steel specimen including an iron carbonate film. Exposed for 10 hours at  $T=80^{\circ}\text{C}$ ,  $\text{pH } 6.6$ ,  $P_{\text{CO}_2} = 0.54 \text{ bar}$ ,  $c_{\text{Fe}^{2+}} = 250 \text{ ppm}$ ,  $v=1 \text{ m/s}$ .

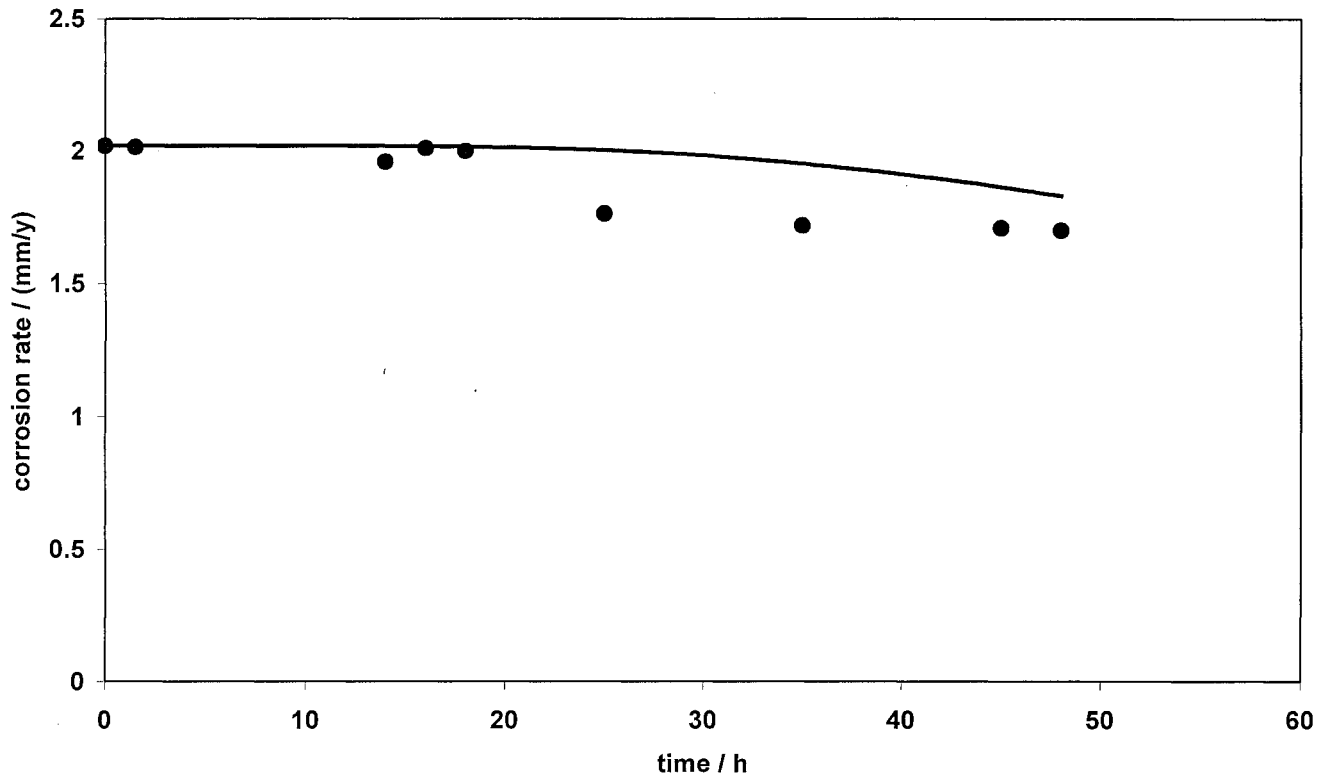


Figure 7. Comparison between experimental data (points) and model predictions (line) for  $T=80^{\circ}\text{C}$ ,  $\text{pH}$  6.6,  $P_{\text{CO}_2} = 0.54$  bar,  $c_{\text{Fe}^{2+}} = 5$  ppm,  $v=1$  m/s.

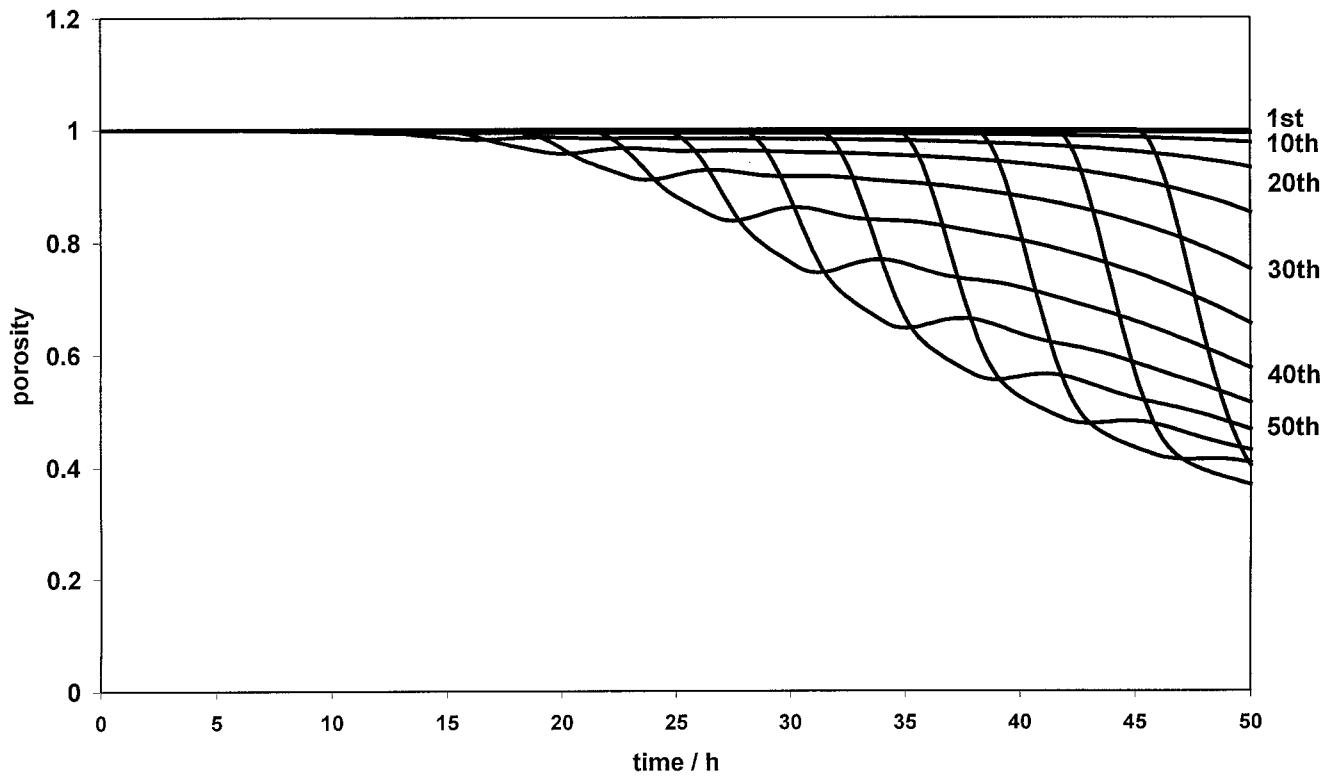


Figure 8. The predicted porosity change of different iron carbonate film layers with respect to time. Each layer is  $0.16 \mu\text{m}$  thick. Conditions:  $T=80^\circ\text{C}$ ,  $\text{pH } 6.6$ ,  $P_{\text{CO}_2} = 0.54 \text{ bar}$ ,  $c_{\text{Fe}^{2+}} = 5 \text{ ppm}$ ,  $v=1 \text{ m/s}$ .

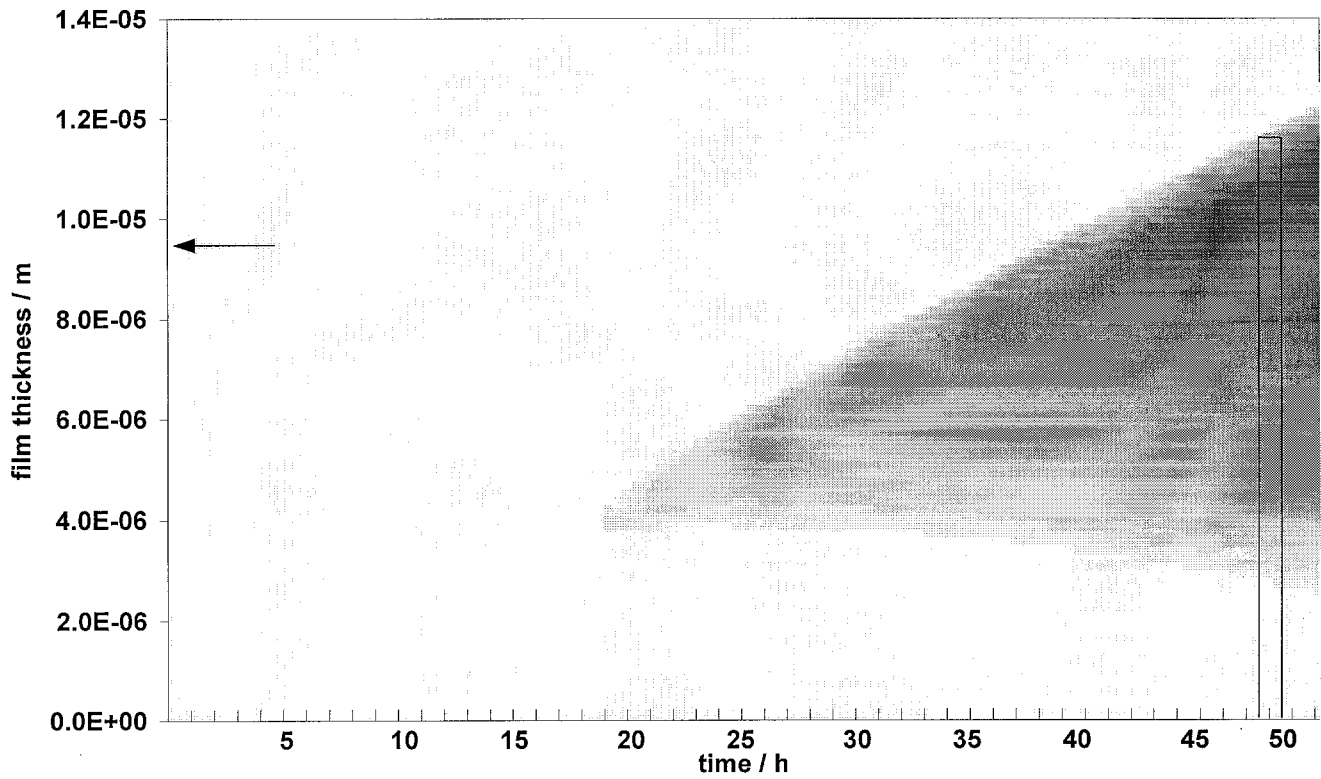


Figure 9. Predicted iron carbonate film growth with respect to time for  $T=80^{\circ}\text{C}$ ,  $\text{pH } 6.6$ ,  $P_{\text{CO}_2} = 0.54 \text{ bar}$ ,  $c_{\text{Fe}^{2+}} = 5 \text{ ppm}$ ,  $v=1 \text{ m/s}$ . Black depicts a 100% dense ( $\varepsilon=0$ ) iron carbonate film and white means no film ( $\varepsilon=1$ ). The arrow denotes the position of the steel surface at the beginning of the corrosion process ( $t=0$ ). The rectangle highlights the film obtained after 48 hours which is used for comparison with the experimentally observed film shown in Figure 10.



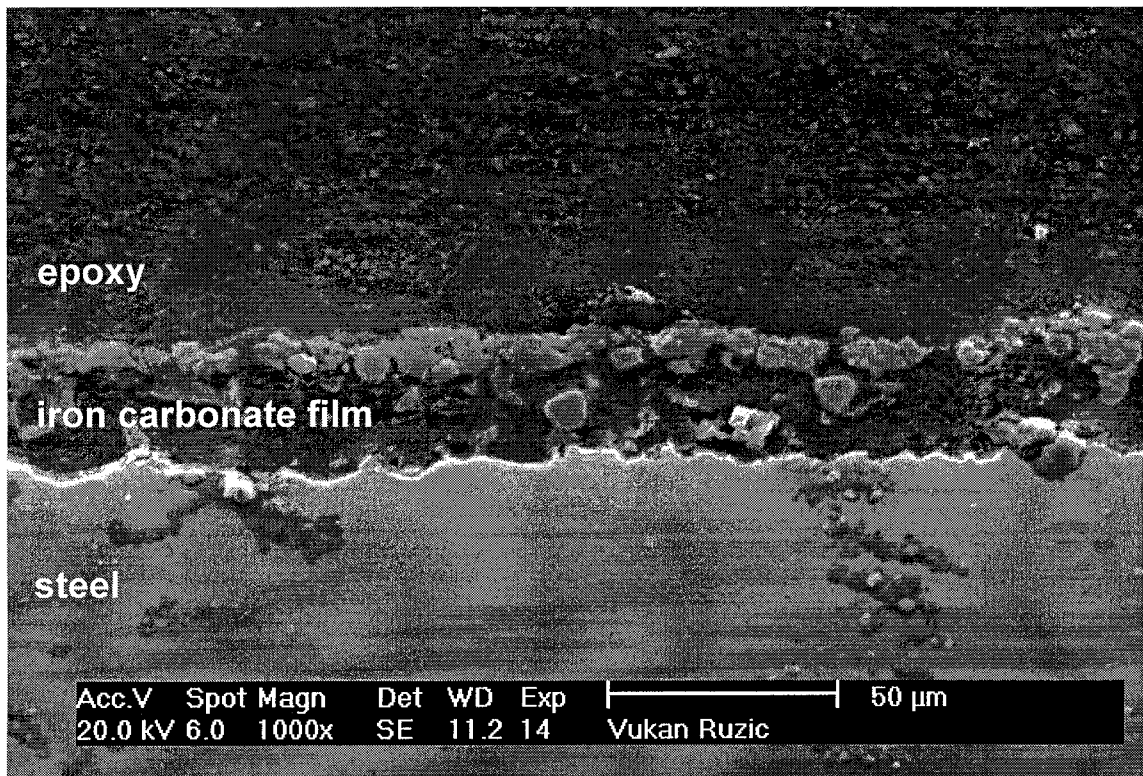


Figure 10. SEM image of a cross section of a steel specimen including an iron carbonate film. Exposed for 48 hours at  $T=80^{\circ}\text{C}$ ,  $\text{pH } 6.6$ ,  $P_{\text{CO}_2} = 0.54 \text{ bar}$ ,  $c_{\text{Fe}^{2+}} = 5 \text{ ppm}$ ,  $v=1 \text{ m/s}$ .

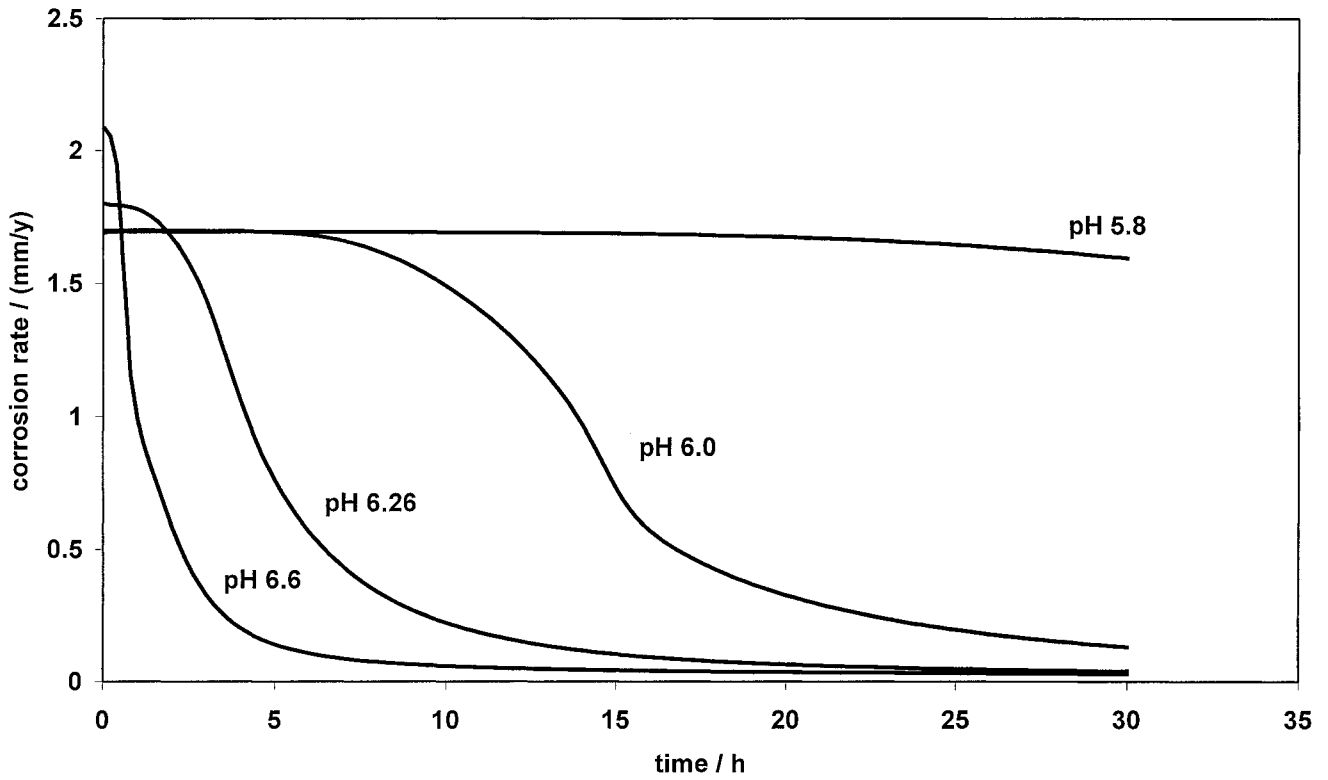


Figure 11. The predicted effect of pH on the corrosion rate for  $T=80^{\circ}\text{C}$ ,  $P_{\text{CO}_2}=0.54$  bar,  $c_{\text{Fe}^{2+}}=250$  ppm,  $v=1$  m/s. Corresponding film thickness and porosity are shown in Figure 12. Predicted supersaturation and scaling tendency are listed in TABLE 1.

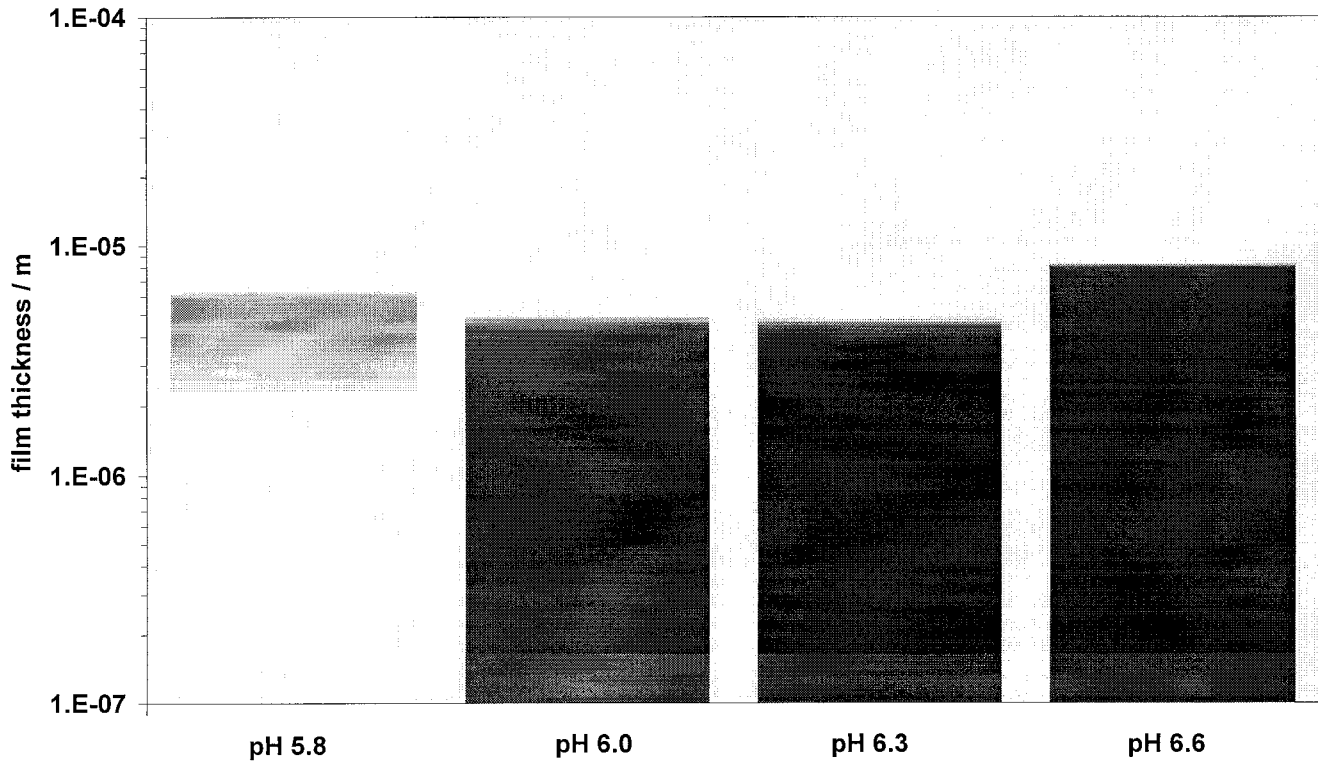


Figure 12. The predicted film thickness and porosity as a function of pH after 30 hours of exposure at  $T=80^{\circ}\text{C}$ ,  $P_{\text{CO}_2}=0.54$  bar,  $c_{\text{Fe}^{2+}}=250$  ppm,  $v=1$  m/s. Black depicts a 100% dense ( $\varepsilon=0$ ) iron carbonate film and white means no film ( $\varepsilon=1$ ). The corresponding corrosion rate curves are shown in Figure 11. Predicted supersaturation and scaling tendency are listed in TABLE 1.

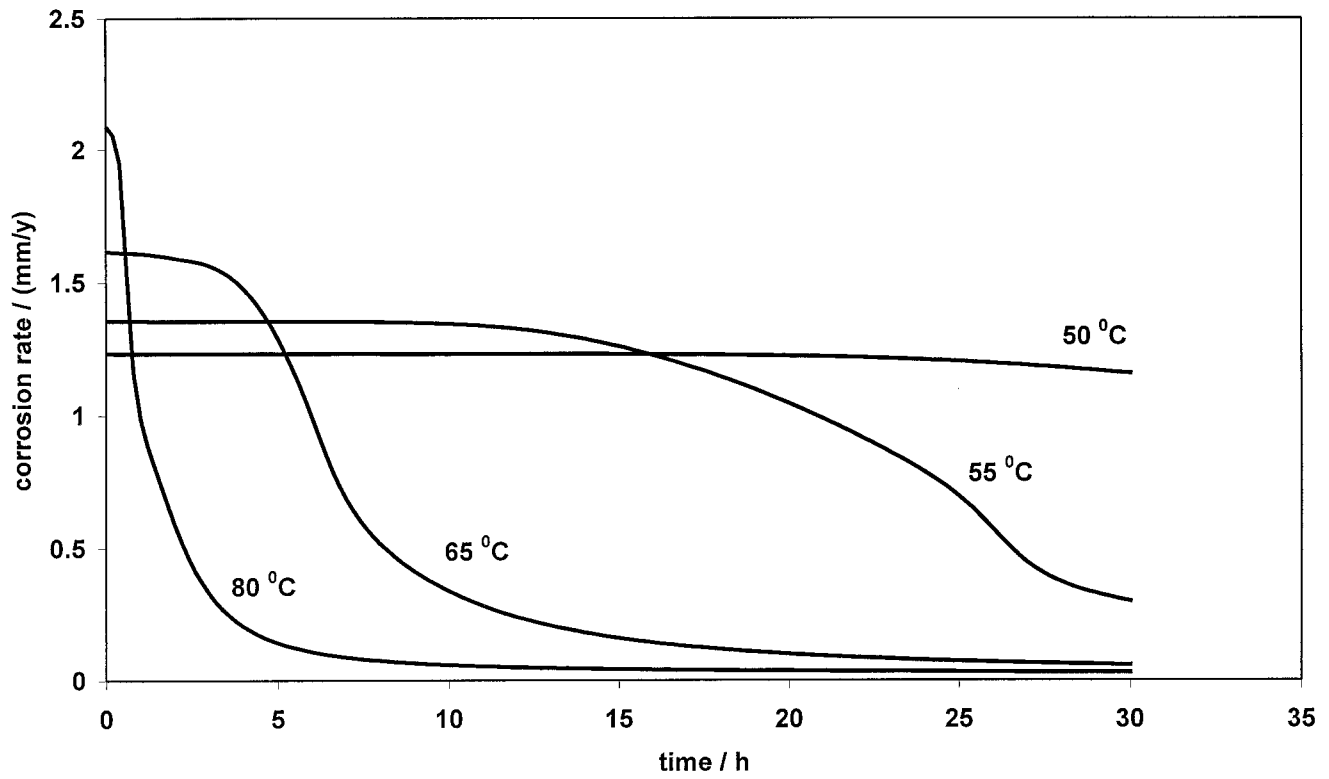


Figure 13. The predicted effect of temperature on the corrosion rate for pH 6.6,  $P_{CO_2} = 0.54$  bar,  $c_{Fe^{2+}} = 250$  ppm,  $v=1$  m/s. Corresponding film thickness and porosity are shown in Figure 14. Predicted supersaturation and scaling tendency are listed in TABLE 2.

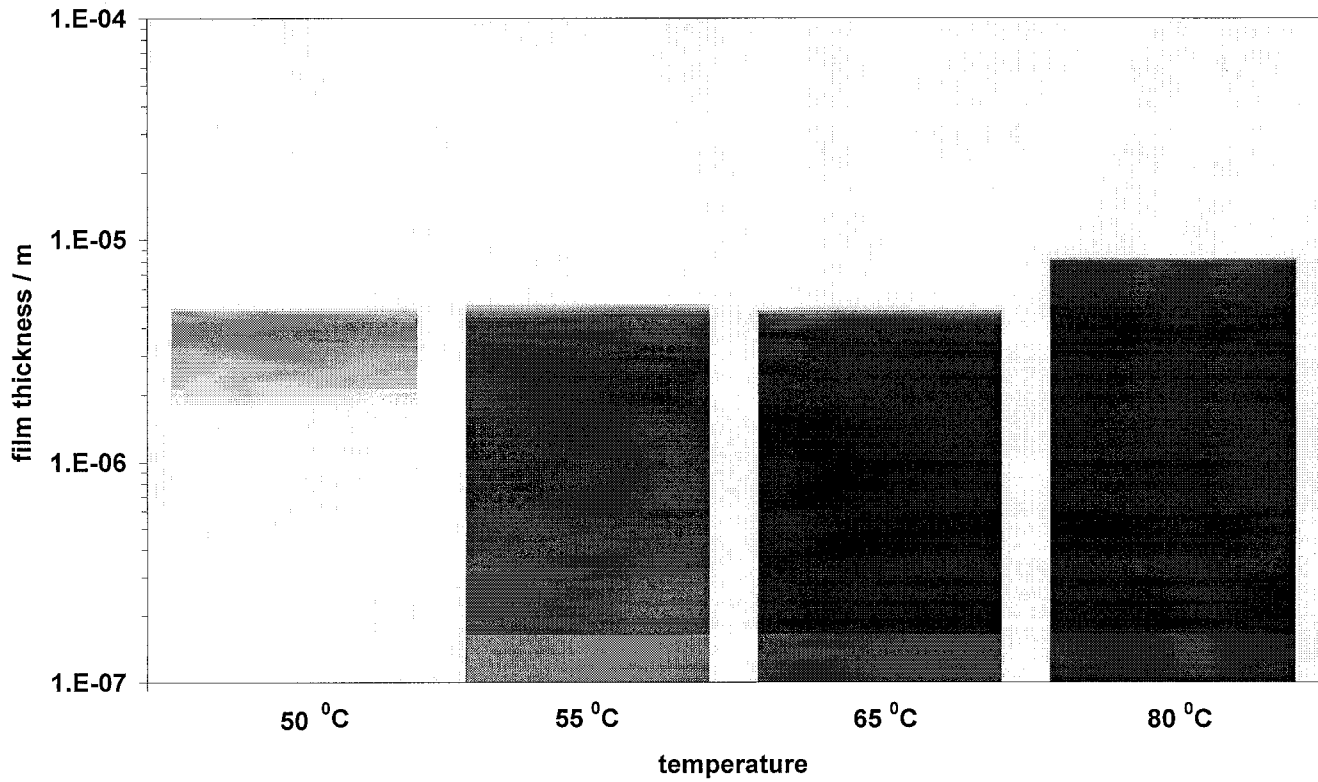


Figure 14. The predicted film thickness and porosity as a function of temperature after 30 hours of exposure at pH 6.6,  $P_{CO_2} = 0.54$  bar,  $c_{Fe^{2+}} = 250$  ppm,  $v = 1$  m/s. Black depicts a 100% dense ( $\varepsilon = 0$ ) iron carbonate film and white means no film ( $\varepsilon = 1$ ). The corresponding corrosion rate curves are shown in Figure 13. Predicted supersaturation and scaling tendency are listed in TABLE 2.

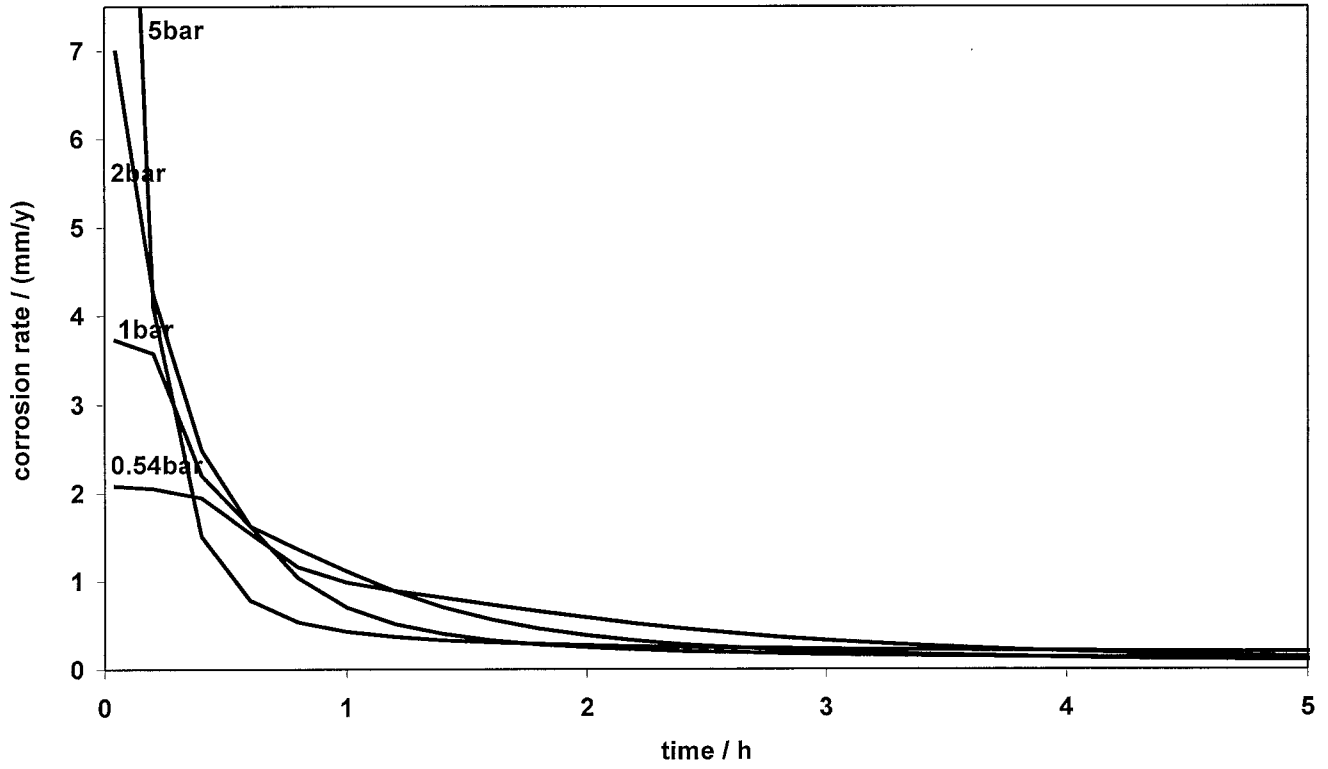


Figure 15. The predicted effect of CO<sub>2</sub> partial pressure on the corrosion rate for T=80°C, pH 6.6,  $c_{Fe^{2+}} = 250$  ppm,  $v=1$  m/s. Corresponding film thickness and porosity are shown in Figure 16. Predicted supersaturation and scaling tendency are listed in TABLE 3.

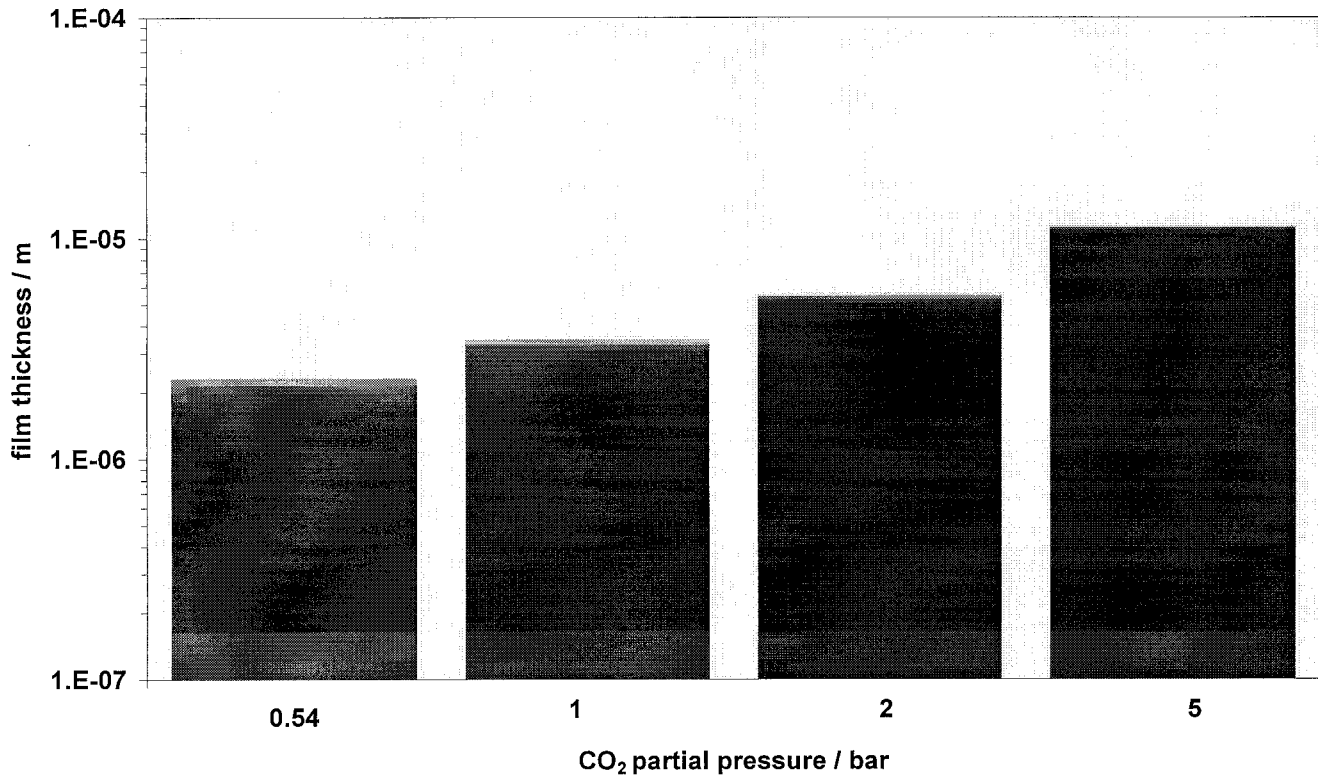


Figure 16. The predicted film thickness and porosity as a function of CO<sub>2</sub> partial pressure after 5 hours of exposure at T=80°C, pH 6.6,  $c_{Fe^{2+}}=250$  ppm,  $v=1$  m/s. Black depicts a 100% dense ( $\epsilon=0$ ) iron carbonate film and white means no film ( $\epsilon=1$ ). The corresponding corrosion rate curves are shown in Figure 15. Predicted supersaturation and scaling tendency are listed in TABLE 3.

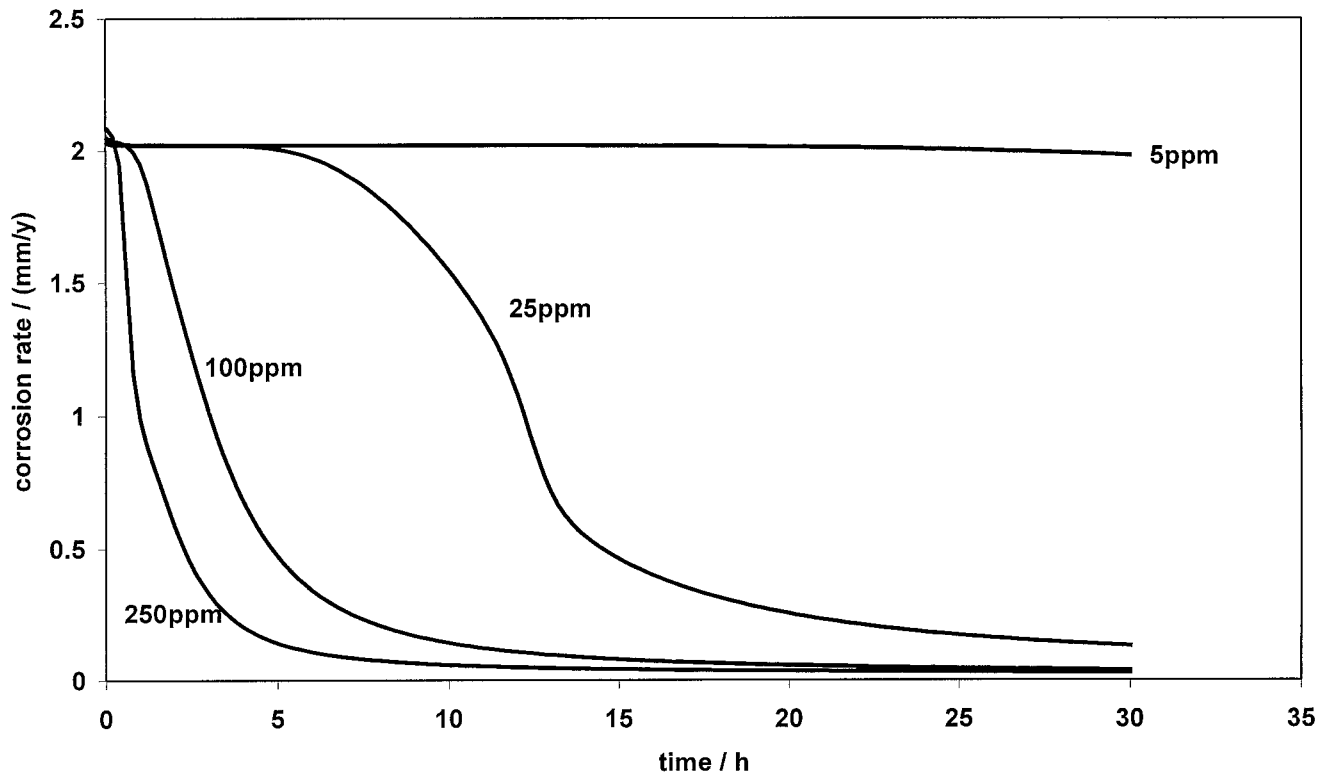


Figure 17. The predicted effect of  $\text{Fe}^{2+}$  concentration on the corrosion rate for  $T=80^\circ\text{C}$ ,  $\text{pH } 6.6$ ,  $P_{\text{CO}_2} = 0.54 \text{ bar}$ ,  $v=1 \text{ m/s}$ . Corresponding film thickness and porosity are shown in Figure 18. Predicted supersaturation and scaling tendency are listed in TABLE 4.



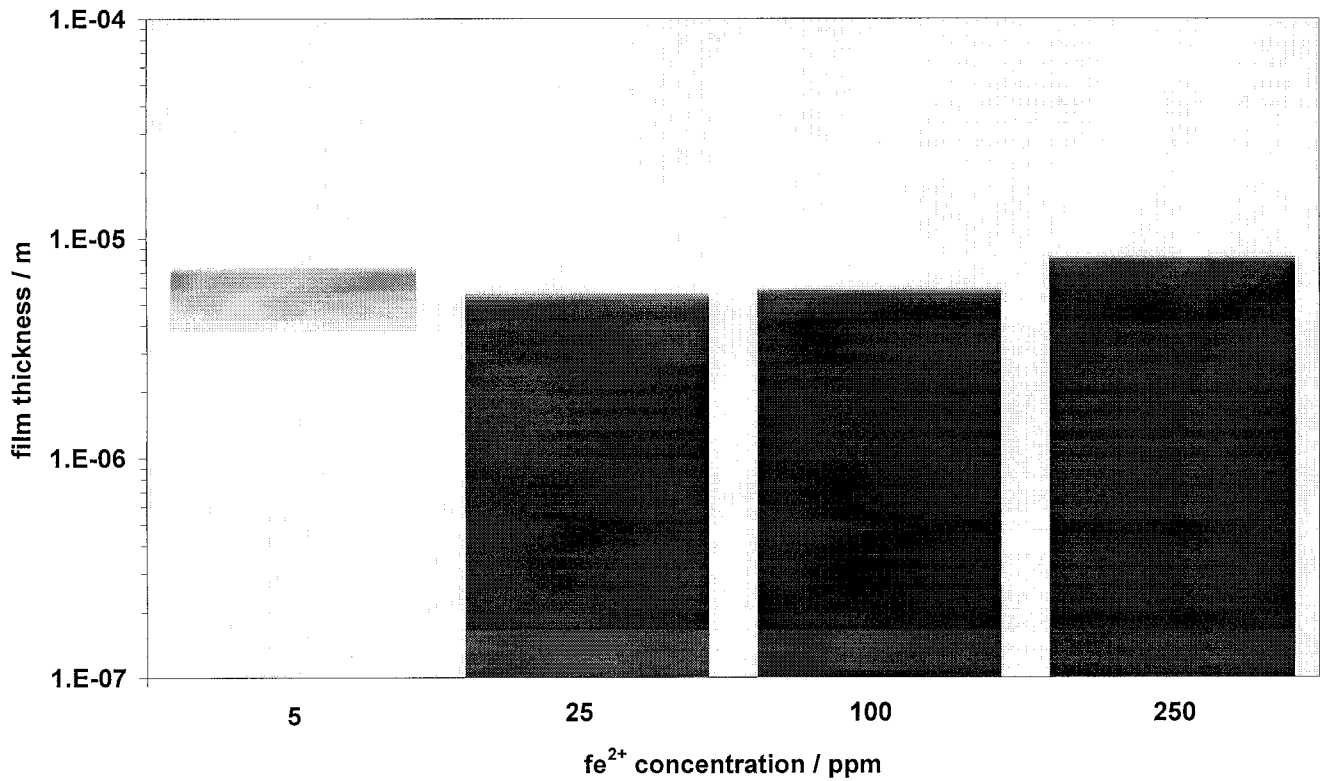


Figure 18. The predicted film thickness and porosity as a function of Fe<sup>2+</sup> ion concentration after 30 hours of exposure at T=80°C, pH 6.6,  $P_{CO_2}$  =1 bar, v=1 m/s. Black depicts a 100% dense ( $\epsilon=0$ ) iron carbonate film and white means no film ( $\epsilon=1$ ). The corresponding corrosion rate curves are shown in Figure 17. Predicted supersaturation and scaling tendency are listed in TABLE 4.

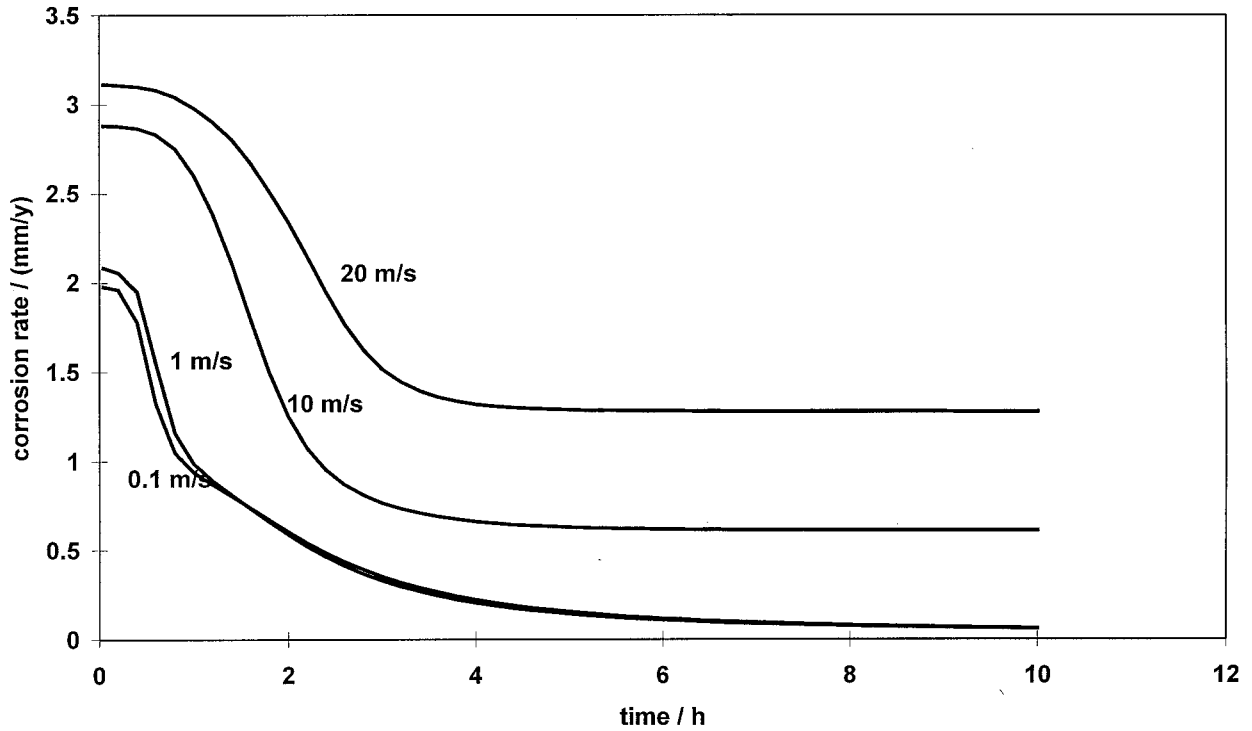


Figure 19. The predicted effect of velocity on the corrosion rate for  $T=80^{\circ}\text{C}$ ,  $\text{pH } 6.6$ ,  $P_{\text{CO}_2}=1 \text{ bar}$ ,  $c_{\text{Fe}^{2+}}=250 \text{ ppm}$ . Corresponding film thickness and porosity are shown in Figure 20. Predicted supersaturation and scaling tendency are listed in TABLE 5.

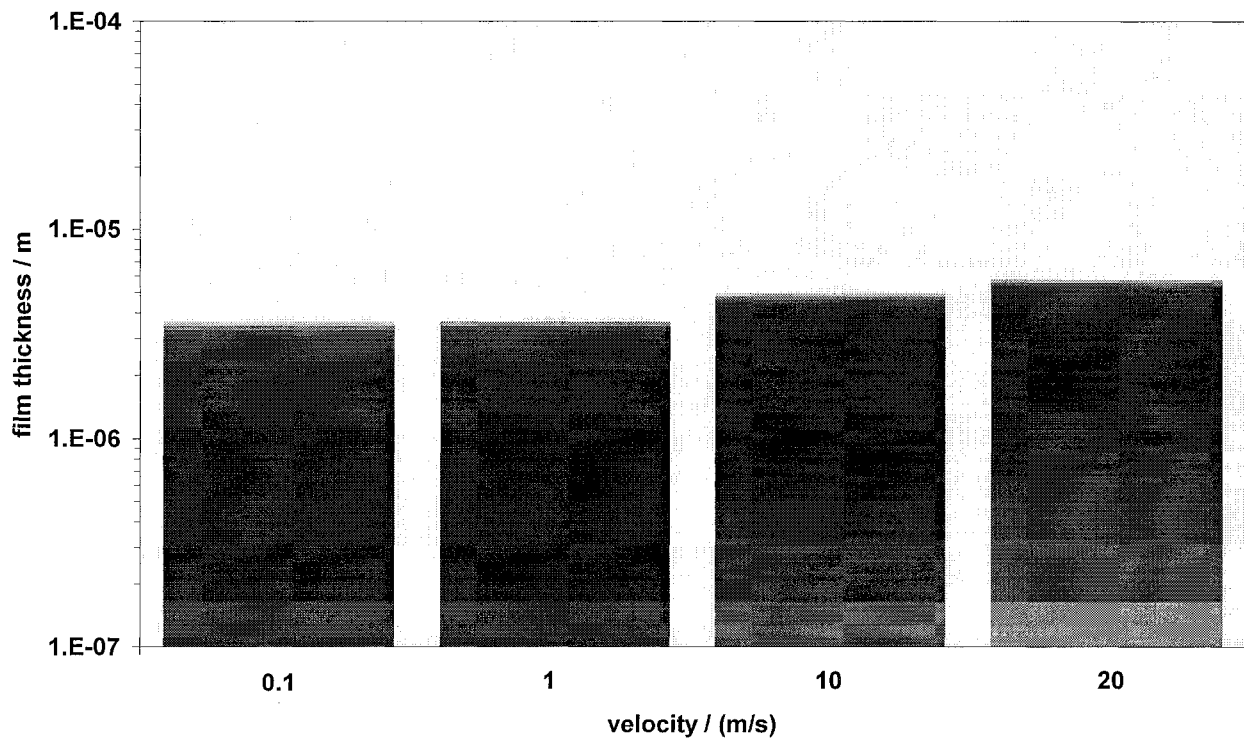


Figure 20. The predicted film thickness and porosity as a function of velocity after 10 hours of exposure at  $T=80^{\circ}\text{C}$ ,  $\text{pH } 6.6$ ,  $P_{\text{CO}_2}=1 \text{ bar}$ ,  $c_{\text{Fe}^{2+}}=250 \text{ ppm}$ . Black depicts a 100% dense ( $\varepsilon=0$ ) iron carbonate film and white means no film ( $\varepsilon=1$ ). The corresponding corrosion rate curves are shown in Figure 19. Predicted supersaturation and scaling tendency are listed in TABLE 5.